Biomedicine & Pharmacotherapy 193 (2025) 118759

Contents lists available at ScienceDirect

Biomedicine & Pharmacotherapy

journal homepage: www.elsevier.com/locate/biopha

# Vutiglabridin ameliorates obesity by directly reducing fat mass through AMPK/lipophagy activation in adipocytes

Hyeong Min Lee [a,c], Jae Ho Lee [a], Sang Hyo Kim [a], Kamindu Gayashan Marakkalage [a], Jihyeon Hur [c], Hyung Soon Park [a], Kwang Pyo Kim [c,d], Gu-Choul Shin [b,*], Sang-Ku Yoo [a,*,1]

[a] Glaceum Inc., Suwon, Republic of Korea
[b] Department of Microbiology, College of Medicine, The Catholic University of Korea, Seoul 06591, Republic of Korea
[c] Department of Applied Chemistry, Institute of Natural Science, Global Center for Pharmaceutical Ingredient Materials, Kyung Hee University, Yongin 446-701, Republic of Korea
[d] Department of Biomedical Science and Technology, Kyung Hee Medical Science Research Institute, Kyung Hee University, Seoul 02453, Republic of Korea

ARTICLE INFO

*Keywords:*
Vutiglabridin
Obesity
Adipocytes
PON2
AMPK
Lipophagy

ABSTRACT

Current anti-obesity therapies that suppress appetite often cause undesirable reductions in lean mass by indirectly depleting systemic energy store. In this study, we developed a novel anti-obesity drug, Vutiglabridin (VUTI), designed to selectively reduce fat mass while preserving lean mass. We evaluated its efficacy in high-fat diet–induced obese (DIO) mice and investigated its underlying mechanism in *in vitro* adipocyte models. VUTI dose-dependently and selectively decreased fat mass, resulting in normalization of body weight within 3 weeks while preserving lean mass. Pharmacokinetic and mechanistic analyses revealed that VUTI targets white adipose tissue (WAT), where it enhances lipid degradation through AMPK-mediated lipophagy in both mouse and human adipocytes. The lipid degradation-enhancing effect of VUTI was shown to be dependent on paraoxonase 2 (PON2). Multi-omics analyses, including proteomic and transcriptomic profiling of epididymal WAT in DIO-mice, further confirmed this mechanism. Collectively, these findings demonstrate that VUTI represents a promising therapeutic strategy for obesity by inducing fat-selective reduction via AMPK-mediated lipophagy.

## 1. Introduction

Obesity is a pathological condition primarily driven by an abnormal or excessive accumulation of body fat [1]. Excessive fat accumulation promotes chronic inflammation and insulin resistance through abnormal secretion of adipokines and pro-inflammatory cytokines, ultimately acting as a major cause of various complications such as type 2 diabetes, cardiovascular diseases and some types of cancer [2,3]. Accordingly, obesity requires therapeutic approaches that selectively reduce fat, which serves as the primary cause of various complications.

Over the past decades, a wide range of pharmacological interventions have been developed to induce weight loss, with the majority targeting appetite suppression to reduce caloric intake. Appetite-suppressing drugs that act via central nervous system (CNS) stimulation, such as phentermine, are frequently associated with significant adverse effects, including cardiovascular, psychiatric, and gastrointestinal complications [4,5]. Despite their safety concerns, these drugs provide only modest weight loss, which substantially limits their clinical utility and long-term acceptability. The emergence of glucagon-like peptide-1 receptor agonists (GLP-1RAs), particularly semaglutide, has shifted the therapeutic landscape in obesity by demonstrating effective weight loss [6]. However, due to their appetite suppressing mechanism

*Abbreviations:* ACC, Acetyl-CoA carboxylase; ATGL, Adipose triglyceride lipase; ATG3, Autophagy related 3; BAT, Interscapular brown adipose tissue; BECN1, Beclin-1; CLS, Crown-like structure; DAG, Diacylglycerols; Epi-fat, epididymal fat; FA, Fatty acid; GAS, Gastrocnemius muscle; HDL, High-density lipoprotein; HFD, High-fat diet; HSL, Hormone-sensitive lipase; Ing-fat, Inguinal-fat; LD, Lipid droplet; LDL, Low-density lipoprotein; LPS, Lipopolysaccharide; MAG, Monoacylglycerols; MDA, Malondialdehyde; MOA, Mechanism of action; NBT, Nitro blue tetrazolium; ORO, Oil Red O; PGC-1, Peroxisome proliferator-activated receptor-gamma coactivator-1; PON2, Paraoxonase 2; QD, Quadriceps muscle; QWBA, Quantitative whole body autoradiography; Retro-fat, Retroperitoneal fat; ROS, Reactive oxygen species; Sema, Semaglutide; TAG, Triacylglycerol; VUTI, Vutiglabridin; WAT, White adipose tissue.

* Corresponding authors.
*E-mail addresses:* rnelr@naver.com (G.-C. Shin), skyoo@glaceum.com (S.-K. Yoo).
[1] Lead contact

https://doi.org/10.1016/j.biopha.2025.118759
Received 31 August 2025; Received in revised form 25 October 2025; Accepted 7 November 2025
Available online 15 November 2025

of action, GLP-1RAs still have some adverse events. Approximately 40 % of the weight loss achieved with semaglutide is derived from a reduction in lean body mass, raising concerns regarding skeletal muscle loss [6]. Although substantial weight loss is achieved during the early phase of treatment, body weight reduction typically plateaus after approximately 1 year, and rapid weight regain is often observed following treatment discontinuation [7,8], suggesting that the long-term efficacy of GLP-1RAs may be limited.

Similarly, caloric restriction (CR) is accompanied by comparable adverse effects, including loss of muscle mass and a weight loss plateau. In general, energy deficiency induced by CR promotes the loss of lean mass, particularly skeletal muscle, via enhanced catabolism of muscle proteins that serve as a source of essential amino acids for gluconeogenesis and protein synthesis [9,10]. Furthermore, while lipolysis is initially upregulated during caloric restriction, prolonged adaptation to nutrient deficiency leads to an impairment in fat reduction capacity [11,12]. In previous study, CR maintained for over 12 weeks led to a reduction in both mRNA and protein expression levels of hormone-sensitive lipase (HSL) and adipose triglyceride lipase (ATGL) in adipose tissue [13]. Recently, increasing evidence suggests that impaired lipolytic capacity in adipocytes also plays a critical role in the progression of obesity [13–15]. In obese individuals, lipogenesis-related processes are upregulated, while lipolysis-related processes are concurrently downregulated, thereby promoting the maintenance of an excessive fat accumulation state [16,17]. Therefore, effective management of obesity requires therapeutic strategies that specifically promote fat mass reduction, addressing the underlying excess adiposity rather than merely reducing total body weight.

Glabridin, an isoflavan found in Glycyrrhiza glabra extract, has been identified as a potential therapeutic candidate for various metabolic diseases, including hyperlipidemia, diabetes, and obesity [18–20]. In animal models, glabridin led to significant reductions in visceral fat mass and adipocyte size, indicating its potential in alleviating obesity [20]. However, its low chemical stability under various physical conditions limits its druggability and clinical applicability [21]. Vutiglabridin (VUTI) is a synthetic derivative of glabridin, developed to improve its chemical stability and oral bioavailability. Recently, we reported the therapeutic efficacy of VUTI in high-fat diet (HFD)-induced obese mice, demonstrating a significant reduction in body weight [22]. However, the underlying anti-obesity mechanism of action (MOA) of VUTI remains to be fully elucidated. In this study, we investigated the tissue distribution and therapeutic effects of VUTI across various adipose and peripheral tissues to identify the primary target organs of its action. Furthermore, through *in vitro* functional studies, we validated the molecular mechanism underlying VUTI-induced lipolysis in adipocytes as well as in the adipose tissue of DIO mice. These findings suggest that VUTI is a novel anti-obesity agent that directly promotes fat reduction in adipocytes.

## 2. Materials and methods

### 2.1. Preparation of Vutiglabridin (VUTI) and reagents

Vutiglabridin, Vutiglabridin-d11, $^{14}$C-labeled Vutiglabridin ([$^{14}$C] VUTI) and 5-thiobutyr-olactone (TBBL) were prepared at Glaceum Inc. (Suwon, Republic of Korea) following the protocols from Patent US9783551B2 [23]. Oil Red O solution (O1391), 5,5′-dithiobis (2-nitrobenzoic acid) (DTNB, D8130), dithiothreitol (DTT, D9776), iodoacetamide (I6125), triethylammonium bicarbonate (TEAB, 18597), formic acid (695076), trifluoroacetic acid (91707), Dexamethasone (D1756), 3-Isobutyl-1-methylxanthine (IBMX; I5879), Insulin (I9278), AMPK inhibitor compound C (171260), and Dimethyl Sulfoxide (DMSO; D2650) were purchased from Sigma-Aldrich. All stock solutions were prepared according to the manufacturer`s instructions.

Details of other materials and suppliers were provided in the supplementary materials.

### 2.2. Quantitative whole-body autoradiography (QWBA)

To investigate the tissue distribution of VUTI in the body, a quantitative whole-body autoradiography assay was performed as previously described [24]. The study protocol was approved by the Institutional Animal Care and Use Committee (IACUC: 2017–016). Male *Sprague Dawley* rats (n = 3, 16 h-fasted; Charles River Laboratories Japan Inc., Yokohama, Japan) of 8 weeks of age were administered 10 mg/kg of [$^{14}$C] VUTI equivalent to radioactivity of 3.7 MBq/kg through oral gavage. After 2, 6, and 24 h, each rat was euthanized by $CO_2$ inhalation. Its nasal cavity and anus were filled with 4 % w/v CMC-Na, and the carcass was subsequently frozen in a dry ice-acetone mixture. A 30 μm thick whole-body sagittal sections were cut with a cryomicrotome (CM3600, Leica Biosystems, Wetzlar, Germany), freeze-dried and covered with 4-μm thick protective membrane (Diafoil, Mitsubishi Plastics, Tokyo, Japan) for 24 h in a sealed lead box along with the plastic standard samples (CFQ7601, Amersham Biosciences Corp., NJ, USA) for calibration. The radioactivity was measured by the bio-imaging analyzer system (FUJI-BAS2500, FUJIFILM, Tokyo, Japan; resolution μm, gradation 256, sensitivity 10000, latitude 4) where the radioactivity in organs was converted to the photo-stimulated luminescence per unit area (PSL/mm2) with the background radioactivity of the plastic standard samples subtracted. Tissue radioactivity in the whole-body autoradiograms was quantified by densitometry using MCID image analysis software (v7.0, MCID Image Analysis Software Solutions for Life Sciences, Cambridge, UK). Radioactivity concentrations were expressed as ng equivalents of [$^{14}$C] VUTI per gram of tissue (ng eq/g tissue).

### 2.3. Quantification of drug concentration in the plasma and adipose tissue of mice

For quantification of dose-dependent changes in plasma concentrations of VUTI, male C57BL/6J mice (8 week-old, n = 6, non-fasted; Charles River Laboratories Japan Inc. and OrientBio, Seongnam, Korea) were orally administered VUTI at doses of 10, 30, or 100 mg/kg. Blood samples were collected at 0, 1, 2, 4, 6, 8, 10, and 24 h after drug administration. Their whole blood was collected via the vena cava in a heparin-coated syringe (n = 3 per time point) and subsequently centrifuged to obtain plasma. The plasma (10 μL) sample was put into a 1.5 mL tube and mixed with 30 μL internal standard solution (1000 ng/mL of Vutiglabridin–d11 in acetonitrile). The tube was vortexed and centrifuged at 13,200 rpm for 5 min at room temperature. The supernatant was transferred to an LC vial and analyzed using an Agilent 6490 Triple Quadrupole UPLC-MS/MS system (Agilent, Santa Clara, California, USA) equipped with an electrospray ionization source. Mass detection was performed in the negative ion mode, and the column temperature was maintained at 40°C using a thermostatically controlled column oven. The column used for the separation was CHIRALPAK IA-3 (1.6 μm, 2.1 × 150 mm). The mobile phases consisted of $H_2O$ (solvent A) and acetonitrile (solvent B), with isocratic elution performed at a flow rate of 0.5 mL/min while maintaining solvent B at 56 %. For multiple reaction monitoring (MRM) analyses, the target ions used were 353.3/137.1 *m/z* for Vutiglabridin and 363.9 /182.9 *m/z* for Vutiglabridin-d11. This study was performed in accordance with the Association for Assessment and Accreditation of Laboratory Animal Care International (AAALAC; Approval No. LCDI-2021–0027).

For the quantification of VUTI in plasma and adipose tissue, Male C57BL/6J mice (8 week-old, n = 24, non-fasted; Charles River Laboratories Japan Inc. and OrientBio, Seongnam, Korea) were dosed with 50 mg/kg of VUTI once and sacrificed at 0, 1, 2, 4, 6, 8, 10, 24-h time points (n = 3 per time point). Their whole blood was collected via the vena cava in a heparin-coated syringe and their adipose tissue (epididymal fat) was collected after perfusion with 0.9 % saline. Using the same analytical method as for plasma, VUTI was extracted from adipose tissues (10 mg) after mixing with 30 μL of internal standard solution (1000 ng/mL of Vutiglabridin–d11 in acetonitrile) and analyzed by LC-

MS. This study was performed in accordance with the Association for Assessment and Accreditation of Laboratory Animal Care International (AAALAC; Approval No. P241005). Detailed pharmacokinetic analyses are described in the Supplementary methods.

### 2.4. Animals model and drug treatment

All animal experiments were conducted in accordance with internationally accepted principles for the care and use of laboratory animals. The license for conducting animal experiments was issued by the Lee Gil Ya Cancer and Diabetes Institute at Gachon University, in compliance with the standards of Association for Assessment and Accreditation of Laboratory Animal Care International (Approval No. LCDI-2019–0176 and LCDI-2018–0133). Male C57BL/6J mice aged 6 weeks (Jackson Labs, USA) were fed a high-fat (60 % kcal fat) (D12492, Research Diets, USA) or normal diet (10 % kcal fat; PicoLab5053, LabDiet, USA). At 14 weeks of age, the mice were acclimatized for 1 week in a controlled environment (12 h light/dark cycle, lights on at 7:00 a.m., 22 ± 2°C, 50 ± 10 % humidity, *ad libitum* access to water and their respective diets) and were randomly divided into groups ensuring that the mean body weights of the obese groups were equivalent. Then, the animals underwent a 2-week administration adaptation period before dosing. At 17 weeks of age, the animals were dosed orally via gastric intubation (50 or 100 mg/kg) for VUTI once a day for 9 days (short-term effect) or 6 weeks (long-term effect). At the end of the study, animals were fasted for 14–16 h and anesthetized by isoflurane inhalation at terminal sacrifice. Animals were housed in individually ventilated cages (IVC Rack System, 13 ×34 ×14 cm, UREATAC, Changwon, Republic of Korea).

### 2.5. Body weight and body composition analysis

Individual food consumption and body weight were monitored daily during the treatment period. Whole-body fat and lean mass were measured on day 28 of administration using an NMR analyzer (Minispec LF-90II, Bruker Optics GmbH, Bruker Corporation, Billerica, MA, USA) that measures both $^{1}H$ and $^{19}F$ in unanesthetized animals within 5 min. To analyze the body composition parameters at the end of the study period, the weights of the epididymal fat (Epi-fat), retroperitoneal fat (Retro-fat), inguinal fat, interscapular brown adipose tissue (BAT), kidney, liver, gastrocnemius muscle (GAS), and quadriceps muscle (QD) were determined.

### 2.6. Metabolic analysis

Metabolic analysis was performed during two separate intervals (on days 28–31 of drug administration) using two independent sets of mice (n = 4–5 per group per set). To measure food intake, energy expenditure, and locomotor activity, the Comprehensive Lab Animal Monitoring System (CLAMS; Columbus Instruments, Columbus, OH, USA) was used [25]. Mice were placed in individual CLAMS metabolic chambers one day prior to measurement and acclimated to the environment for 15 h. Metabolic monitoring was initiated and continued for 48 h. Oxygen consumption ($VO_2$), carbon dioxide production ($VCO_2$), and locomotor activity (measured via infrared beam breaks) were recorded at 10-min intervals. Energy expenditure (kcal) was calculated using the formula: Energy expenditure = (3.815 + 1.232 × RER) × $VO_2$. The 10-min interval data were averaged into hourly values. Energy absorption was estimated based on the caloric density of the diets: for the normal diet group, intake (kcal) = average food intake (g) × 3.43 kcal/g; for the high-fat diet (HFD) groups, intake (kcal) = average food intake (g) × 5.24 kcal/g.

### 2.7. Fecal energy excretion

Feces were collected over a 24-h period on day 31 of drug administration. At the time of morning dosing, cages were replaced with clean ones, and all fecal output was collected using forceps over the subsequent 24 h. The wet weight of feces (mg) was measured immediately after collection, and samples were stored in 1.7 mL microcentrifuge tubes at −80 °C until analysis. For calorimetric analysis, fecal samples collected on Day 31 were freeze-dried for 48 h using a lyophilizer. The dry weight (mg) was recorded immediately after drying, and the caloric content of the dry feces was determined using a bomb calorimeter (Parr 6400 Calorimeter; Parr Instrument Company, Moline, IL, USA).

### 2.8. Serum preparation and biochemical analysis

Blood samples were collected at sacrifice from the abdominal vein. The glucose level was measured in the serum using a blood-chemical analyzer (7180, HITACHI, Japan). Serum insulin level was measured by using the Mouse Insulin ELISA Kit, TMB type (MIT-696, Shibayagi Co., Ltd., Japan). Serum leptin level was measured using the Mouse Leptin ELISA Kit, TMB type (MLP-817, Shibayagi Co., Ltd).

### 2.9. Tissue processing and immunohistochemistry

The epididymal adipose tissue was fixed for 12–16 h at room temperature in 10 % formalin, embedded in paraffin, sectioned at 5 μm-thick sections, and mounted on charged glass slides. Slide glasses were deparaffinized in xylene, and stained for expression of F4/80, as previously described [26]. Crown-like structure (CLS) number was defined as a circular region surrounded by F4/80 cells in paraffin sections stained for F4/80. CLS was counted in at least 100 random adipocytes per sample, and the percentage of CLS number/total cell number was used to compare CLS density among lean, HFD, and VUTI-treated HFD. Adipocyte size was measured in the same sections stained for F4/80 and was calculated as the mean diameter of at least 20 random adipocytes per sample.

### 2.10. Cell culture and differentiation

The 3T3-L1 preadipocytes were obtained from the Korean Cell Line Bank (KCLB-10092.1, Seoul, Republic of Korea). The cells were cultured in DMEM (LM001–05, Welgene) supplemented with 10 % bovine calf serum and 100 U/mL of penicillin and streptomycin at 37°C in a 5 % $CO_2$ incubator. The cells between passages 3 and 10 were used for the subsequent experiments. To investigate the effect of VUTI during adipogenesis, preadipocytes were induced to differentiate upon reaching confluence in DMEM including 10 % FBS and MDI (0.5 mM 3-isobutyl-1-methylxanthine, 1 μM dexamethasone and 1 μg/mL insulin) with or without VUTI or DMSO. After 2 days, the medium was replaced with DMEM containing 10 % FBS and 1 μg/mL insulin with or without VUTI or DMSO every 2 days until day 10. To test the effect of VUTI on lipolysis, fully differentiated adipocytes at day 10 induced by MDI were treated with VUTI or DMSO every 2 days until day 14. The undifferentiated cells were maintained in DMEM containing 10 % bovine calf serum. To evaluate the anti-inflammatory properties of VUTI, both VUTI-treated and untreated control cells were challenged with 100 ng/mL of LPS for 24 h. The expression levels of target genes were subsequently assessed by RT-PCR.

The hTERT A41hWAT-adipocyte (hWAT) was obtained from the American Type Culture Collection (CRL-3386, ATCC, Manassas, VA, USA). The cells were cultured in DMEM (LM001–05, Welgene) supplemented with 10 % bovine calf serum and 100 U/mL of penicillin and streptomycin at 37°C in a 5 % $CO_2$ incubator. The cells between passages 3 and 10 were used for the subsequent experiments. To investigate the effect of VUTI during adipogenesis, until confluence, preadipocytes were induced to differentiate in DMEM including 2 % FBS and differentiation media (500 μM Isobutyl-methylxanthine, 5 μM dexamethasone, 10 μg/mL human insulin, 5 nM T3, 30 μM indomethacin, 20 μM pantothenate, 40 μM biotin) with or without VUTI or DMSO. After 9 days, the medium was replaced with DMEM containing 10 % FBS and

1 μg/mL insulin with or without VUTI or DMSO every 2 days until day 15. To test the effect of VUTI on lipolysis, fully differentiated adipocytes at day 15 induced by differentiation media were treated with VUTI or DMSO every 2 days until day 25. The undifferentiated cells were maintained in DMEM containing 10 % bovine calf serum.

### 2.11. Generation of PON2 knockdown cells

Stable PON2 knockdown (KD) human adipocytes were generated by transducing the cells with a recombinant lentivirus vector harboring a short hairpin RNA against PON2 (shPON2; Genecopoeia, LPP-HSH013480-LVRU6P). PON2 KD cells were cultured in DMEM supplemented with puromycin (500 ng•mL$^{-1}$) (A11138–03, Life Technologies). The KD of PON2 was confirmed using immunoblotting with anti-PON2 antibody.

### 2.12. Cytotoxicity assay

For cytotoxicity analysis in human adipocytes, cells were seeded into a 96-well culture plate and were treated with a different concentration of VUTI (7.5, and 10 μM) for 24 h, and MTT (3-(4, 5-dimethylthiazolyl-2)-2, 5-diphenyltetrazolium bromide) solution (5 mg•mL$^{-1}$ of the final concentration) was treated for 2 h. The supernatant was removed from the well, and the precipitate obtained was dissolved in DMSO. The levels of insoluble formazan formation were determined at 570 nm using a SpectraMax Plus 384 Microplate Reader (Agilent Technologies, Seoul, Republic of Korea).

### 2.13. RNA extraction and quantitative RT-PCR

Total RNA was extracted from the adipocyte using TRIzol reagent (T9424, Sigma-Aldrich) and was reverse transcribed using M-MLV reverse transcriptase (27032, iNtRON Biotechnology) and an oligo-dT primer according to the manufacturer`s instructions. Quantitative PCR was performed on a 7500 real-time PCR System (Applied Biosytems) with SYBR Green PCR Master Mix (4309155, Thermo Fisher Scientific) following the manufacturer's protocols. Primers of *IL1B, TNF, IL6*, *CCL2*, and *ACTB* are listed in Supplementary Table S1.

### 2.14. Oil red O (ORO) staining

The cells fixed with 4 % paraformaldehyde for 10 min were stained with ORO solution (O1391, Sigma-Aldrich) for 15 min at room temperature. After washing once with 60 % isopropanol, the cells were rinsed with distilled water. The images were captured using an inverted microscope (Carl Zeiss Axioimager M2 fluorescence microscopy). To quantify the ORO staining, the ORO was eluted with isopropanol, and the staining intensity was measured by absorbance at 510 nm.

### 2.15. TAG assay

To determine intracellular TAG concentration, cells were suspended in 100 μL of PBS with 1 % TritonX-100 and heated to 80 −100°C for 5 min to solubilize the intracellular TAG. After centrifugation at 10,000 ×g at 4°C for 5 min, the supernatant was collected and then the TAG content was measured using a TAG Colorimetric assay kit (Cayman Chemical, MI) according to the manufacturer`s instruction. Absorbance was detected at 540 nm using a microplate reader (BioTeck Instruments Inc.). Protein concentrations were measured using BCA assay kit (23225, Thermo Fisher Scientific) and results are presented as nM TAG per mg protein.

### 2.16. Reactive oxygen species (ROS) assay

The generation levels of ROS in adipocytes were detected using the nitro blue tetrazolium (NBT) assay [27]. On day 10 for adipogenesis study or day 15 for lipolysis study of VUTI, the cells were incubated for 90 min in PBS containing 0.2 % NBT. The dark-blue formazan was dissolved in 50 % acetic acid, and its absorbance was determined at 570 nm.

### 2.17. Lipid peroxidation assay

Lipid peroxidation in the cells was determined by measuring the levels of malondialdehyde (MDA), by indirectly measuring the formation of thiobarbituric acid reactive substances (TBARS), which is a chromogen derived by the reaction of MDA with the thiobarbituric acid reaction. The cells were trypsinized and centrifuged; then, the cell pellets were washed with PBS and stored at −80°C until use. The MDA concentration was determined using the TBARS parameter assay kit (KGE013, R&D systems) following the manufacturer's instructions.

### 2.18. Lipolysis assay

Lipolysis in adipocytes was monitored as described previously [26]. Briefly, lipolysis was assessed from the release of glycerol and fatty acid (FA) in the culture medium and cells using free glycerol reagent (F6428, Sigma-Aldrich) and non-esterified FAs measurement kit (LABNEFA-M1, FUJIFILM Wako Pure Chemical Co.) following the manufacturer's instructions.

### 2.19. Immunoblotting analysis

To extract proteins, the cultured cells were lysed using SDS lysis buffer (100 mM Tris-HCl, pH 6.8, 10 % glycerol, and 1 % SDS), supplemented with protease inhibitor cocktail. The protein concentration was determined using the BCA assay kit (Thermo Fisher Scientific). The samples were boiled in 1 × sample buffer (10 mM Tris-HCl, pH 6.8, 1 % SDS, 5 % glycerol, 0.05 % bromophenol blue, and 1 % β-mercaptoethanol) for 5 min and then subjected to SDS-polyacrylamide gel electrophoresis. The resolved proteins were electro transferred onto an Immobilon-P membrane (IPVH00010, Merck). Finally, the membrane was probed with specific antibodies, and immunoreactive signals were detected using a LAS-4000 Luminescent Image Analyzer (GE HealthCare Technologies Inc.). The signal intensity was assessed by measuring the relative density of each band and normalizing it to that of *ACTB* using the Multi Gauge software (FUJIFILM). All antibodies used in this study are listed in Supplementary Table S2.

### 2.20. Isolation of lipid droplet (LD) fractions and lipophagy marker study

For the isolation of LDs from 3T3-L1 adipocytes, a modified method was used as previously described [28]. Cells were homogenized in LD buffer (20 mM Tris-Cl, pH7.4 and 1 mM EDTA with protease inhibitors) and centrifuged at 1000 ×g at 4°C for 10 min. Supernatants were mixed with OptiPrep (D1556, Sigma-Aldrich) to obtain a suspension of 30 %, which was placed in ultracentrifugation tubes (SW40 tubes; Beckman Coulter GmbH, Germany). This bottom layer was overlaid with 20 % and 10 % OptiPrep mixtures in LD buffer and finally with LD buffer supplemented with protease inhibitors. The gradients were centrifuged at 4°C for 3 h and 40,000 rpm (SW40TI rotor). LD layers on top of the gradient were collected. This fraction was delipidated using four volumes of methanol relative to the sample, the proteins were dried and then solubilized in SDS solubilizing buffer for immunoblotting. Total protein was stained using SYPRO™ Ruby Protein Blot stain reagents (S11791, Thermo Fisher Scientific) as loading control.

### 2.21. Fluorescence microscopy

Cells were fixed and processed for immunofluorescence using standard procedures, as described previously [29]. Briefly, cells were rinsed in PBS, fixed in 4 % paraformaldehyde. Fixed cells were blocked in

buffer containing 5 % bovine serum albumin and serially incubated in anti-LC3B or LAMP1 antibodies and anti-rabbit conjugated Alexa Fluor 488 antibody in blocking buffer. Cells were incubated with HCS LipidTOX Deep Red Neutral Lipid Stain (H34477, Thermo Fisher Scientific) for LD detection and Hoechst 33342 (H3570, Thermo Fisher Scientific) for nucleus staining. Images were acquired using a Carl Zeiss Confocal LSM710 Meta microscope and were processed with the software supplied by the manufacturer. Quantification was performed after appropriate thresholding using NIH ImageJ software on a minimum of 50 cells from at least three independent experiments. Percentage colocalization was calculated using the Java Constraint Programming plugin in single Z-stack sections of deconvolved images.

### 2.22. ATP and AMP levels monitoring

Total ATP and AMP production were measured through an ATP Assay Kit (Abcam, ab83355) and AMP Assay Kit (Abcam, ab273275), respectively. In brief, cells were harvested, washed with PBS, and resuspended in 100 μL of ATP assay buffer or AMP assay buffer. Cells were homogenized and centrifuged at 10,000 ×g at 4°C for 5 min to remove any insoluble material. The supernatants were collected, and the concentration of ATP or AMP were analyzed by each assay kit according to manufacturer`s instruction. Absorbance was measured at 570 nm using a microplate reader (BioTeck Instruments Inc.). Protein concentrations were measured using the BCA assay kit, and results are presented as nM ATP or AMP per mg protein.

### 2.23. Quantification of PON2 enzyme activity

Cells were plated into six-well plates and incubated with presence or absence of 2.5–5 μM VUTI for 72 h. Next, the cells were trypsinized and centrifuged. The cell pellets were washed with PBS and stored at −80°C until use. The frozen cell pellets and liver tissues were incubated with 25 mM Tris buffer (pH 7.4) containing 0.05 % n-dodecyl-β-D-maltoside (D4641, Merck) and 1 mM $CaCl_2$ and lysed by subjecting to three freeze-thaw cycles.

To evaluate the PON2 esterase activity, p-nitrophenyl acetate (pNPA) hydrolysis was determined using a SpectraMax Plus384 microplate reader (Agilent Technologies, Seoul, Republic of Korea). The cell lysates were transferred to a 96-well plate, and reactions (0.2 mL final mixture volume) were initiated by adding 1 mM pNPA in PON2 activity assay buffer (50 mM Tris [pH 8.0] with 1 mM $CaCl_2$). The increase in absorbance at 412 nm resulting from the release of p-nitrophenol was monitored.

To evaluate the PON2 lactonase activity, the enzymatic hydrolysis of the thioalkyl-substituted lactones was determined. The cell and adipose tissue lysates were transferred to a 96-well plate, and reactions were initiated by adding 1 mM 5-thiobutyl butyrolactone (TBBL) and 1 mM 5',5-dithiobis (2-nitrobenzoic acid [DTNB]; Sigma Aldrich, D8130) in PON2 activity assay buffer. The enzymatic hydrolysis was monitored by examining the absorbance of the reaction mixture at 420 nm.

All enzymatic activity of each experiment were normalized by total protein concentration. The protein concentration was determined using the BCA protein assay kit (23225, Thermo Fisher Scientific).

### 2.24. RNA-seq analysis

For RNA-seq analysis, total RNA was extracted from adipose tissues using the RNeasy Kit (Qiagen, Hilden, Germany). RNA quantity and quality were assessed using Qubit (Thermo Fisher Scientific, OR, USA) and a Bioanalyzer (Agilent, Waldbronn, Germany). RNA-seq libraries were prepared with the TruSeq Stranded mRNA Library Kit (Illumina, CA, USA) and sequenced on a NextSeq 500 platform (Illumina). Reads were aligned to the *Mus musculus* GRCm38 v84 reference genome using STAR v2.5.2a, and differential expression analysis was performed with DESeq2.

### 2.25. Proteomic analysis

For proteomic analysis, the method previously used for tissue proteomics was applied [30]. Briefly, adipose tissues were homogenized in 0.5 mL radioimmunoprecipitation assay lysis buffer, and proteins were extracted, quantified, and digested using the S-Trap method. Resulting peptides were labeled with TMT 16-plex reagents, fractionated by high-pH reverse-phase chromatography, and analyzed by LC–MS/MS on a Q Exactive Plus Orbitrap mass spectrometer. Raw data were processed in Proteome Discoverer v2.4 using the Sequest HT search engine against the UniProt mouse FASTA database (Jan 2025, 17,240 entries), with a 1 % FDR at the protein and peptide levels. Differentially expressed proteins (DEPs) were identified using a fold change $\geq 1.2$ and p-value $< 0.05$. Functional analysis was performed to explore Gene Ontology (GO) biological processes (BP) and molecular functions (MF) associated with DEPs.

### 2.26. Statistical analysis

All data, except RNA-seq and proteomic data, were expressed as the means ± standard error with GraphPad Prism (ver. 10 for Windows; GraphPad Software, Inc., San Diego, CA). Data was obtained from at least three independent experiments. Statistical analyses were performed using an unpaired, two-tailed Student's *t*-test. P-values less than 0.05 were considered statistically significant.

## 3. Results

### 3.1. VUTI predominantly distributes in adipose tissue

To investigate the therapeutic target tissue of VUTI, a quantitative whole-body autoradiography (QWBA) analysis [24] was conducted in Sprague-Dawley (SD) rats using [$^{14}$C] VUTI. Following a single administration of 10 mg/kg [$^{14}$C] VUTI, tissue distribution was evaluated and quantified at 2, 6 and 24 h post-dose using whole-body sagittal sections of SD rats. VUTI was detected across multiple organs, including the liver, pancreas, heart, kidney, and skeletal muscle. The maximum plasma concentration ($T_{max}$) of VUTI was observed at 6 h, at which point VUTI exhibited the highest accumulation in adipose tissues (Fig. 1A, S1). Notably, at $T_{max}$, the concentration of VUTI was 11.1-fold higher in brown adipose tissue (BAT) and 10.9-fold higher in white adipose tissue (WAT) than in plasma (Fig. 1B). We further evaluated the tissue distribution of VUTI in C57BL/6J mice. First, to evaluate dose-dependent exposure of VUTI, single oral doses of 10, 30, and 100 mg/kg were administered to C57BL/6J mice. Both the time to $T_{max}$ and the total area under the concentration-time curve ($AUC_{0–24h}$) increased proportionally with the administered dose (Fig. 1C). Second, to precisely assess the extent of VUTI distribution in adipose tissue relative to plasma, we measured drug concentrations in plasma and white adipose tissue at multiple time points (0, 1, 2, 4, 6, 8, 12, and 24 h) following a single 50 mg/kg oral dose (Fig. 1D). At the Tmax of 10 h, the concentration of VUTI in white adipose tissue was 34.2-fold higher than in plasma (44.5 μg/g vs. 1.3 μg/mL). Based on the $AUC_{0–24h}$ (669.2 μg·h/g in adipose tissue vs. 16.4 μg·h/mL in plasma), the drug exposure in adipose tissue was approximately 40.8-fold greater than in plasma. These findings consistently confirm that VUTI predominantly distributes in adipose tissue.

### 3.2. VUTI preferentially reduces fat mass in HFD-induced obese mice

VUTI showed increased plasma exposure without accumulation up to 100 mg/kg (Fig. 1C), and its anti-obesity effects were evaluated at a dose of 100 mg/kg. To evaluate the short-term anti-obesity effects of VUTI, mice were fed a 60 % high-fat diet (HFD) for 11 weeks to establish a classic diet-induced obesity model. Following obesity induction, mice were administered with VUTI 50 mg/kg and semaglutide (Sema) 30

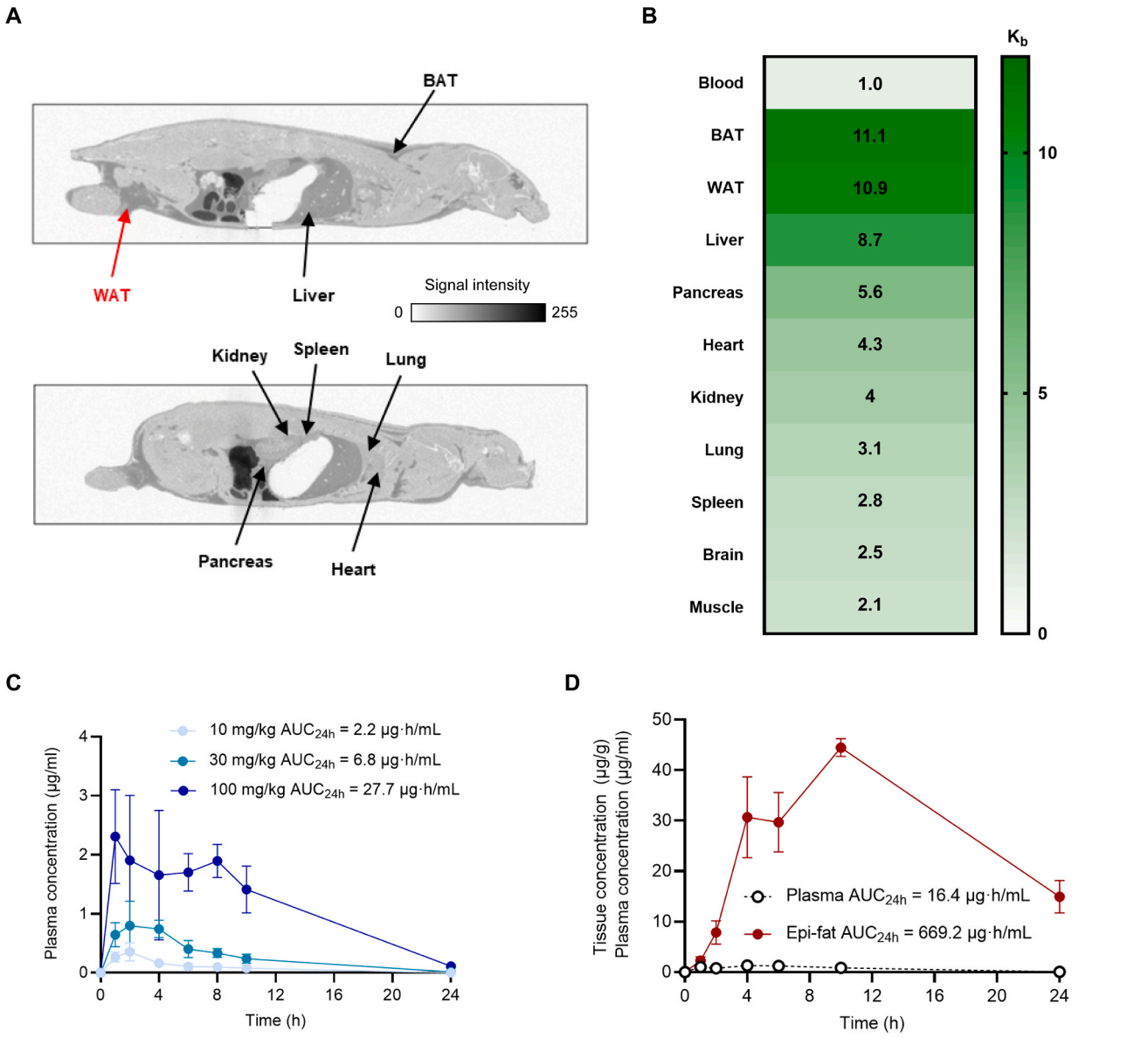


**Fig. 1.** Distribution of Vutiglabridin (VUTI). Quantitative Whole Body Autoradiography (QWBA) in Sprague Dawley (SD) rat and pharmacokinetic analysis of VUTI in mice. (A) Whole-body autoradiograms at 6 h after a single oral administration of 10 mg/kg [$^{14}$C] VUTI to SD-rat. (B) The ratio of radioactivity concentration in each tissue to blood in SD rat. (C) Plasma concentration after single oral administration of 10, 30, 100 mg/kg VUTI to C57BL/6J mice. (D) Plasma and adipose tissue concentration after single oral administration of 50 mg/kg VUTI to C57BL/6J mice. Pharmacokinetic (PK) data are represented as mean ± standard deviation (SD) of 5 animals for each time point. BAT, brown adipose tissue; WAT, white adipose tissue; Epi-fat, epididymal fat.

nmole/kg daily for 9 days (Fig. 2A). In Sema-treated mice, body weight began to decrease immediately after treatment, showing 11.6 % reduction compared to baseline by day 9. In contrast, VUTI-treated mice exhibited no initial change in body weight, but a gradual reduction from day 4, reaching –5.3 % by day 9 (Fig. 2B and C). Due to these distinct patterns of weight loss, dual-energy X-ray absorptiometry (DXA) analysis revealed divergent effects of VUTI and Sema on body composition (Fig. 2D). Sema treatment led to reductions in both lean mass (–6.9 % vs vehicle) and fat mass (–23.7 % vs vehicle), whereas VUTI induced a selective decrease in fat mass (–16.0 % vs vehicle) without affecting lean mass. This fat-selective reduction was consistently observed in individual tissues (Fig. 2E and F). In Sema-treated mice, tissue weight reductions occurred not only in adipose tissues including epididymal fat (Epi-fat), retroperitoneal fat (Retro-fat), inguinal fat (Ing-fat), and interscapular brown adipose tissue (BAT) but also in non-adipose tissues such as the liver, kidney, and muscle tissues including the gastrocnemius (GAS) and quadriceps (QD). In contrast, VUTI-treated mice exhibited reductions in adipose tissue mass (Epi-fat, Retro-fat, and Ing-fat) compared to those observed with Sema-treated mice, while liver and kidney weights remained unchanged. Notably, the muscle tissue weights (GAS and QD) were slightly increased relative to the DIO-vehicle group. These findings suggest that the anti-obesity effect of VUTI is driven by fat-selective loss.

### 3.3. *VUTI dose-dependently reduces fat mass in HFD-induced obese mice*

To investigate the dose-dependent and long-term anti-obesity effects of VUTI, mice were fed a high-fat diet for 11 weeks to induce obesity and then treated daily with VUTI (50 or 100 mg/kg) and Sema (30 nmol/kg) for 6 weeks (Fig. 3A). VUTI-treated mice exhibited a dose-dependent reduction in both body weight and fat mass. Notably, mice treated with 100 mg/kg VUTI showed a progressive decrease in body weight and fat mass, ultimately reaching levels comparable to those of lean controls by week 4, without significant changes in lean mass (Fig. 3B, C,

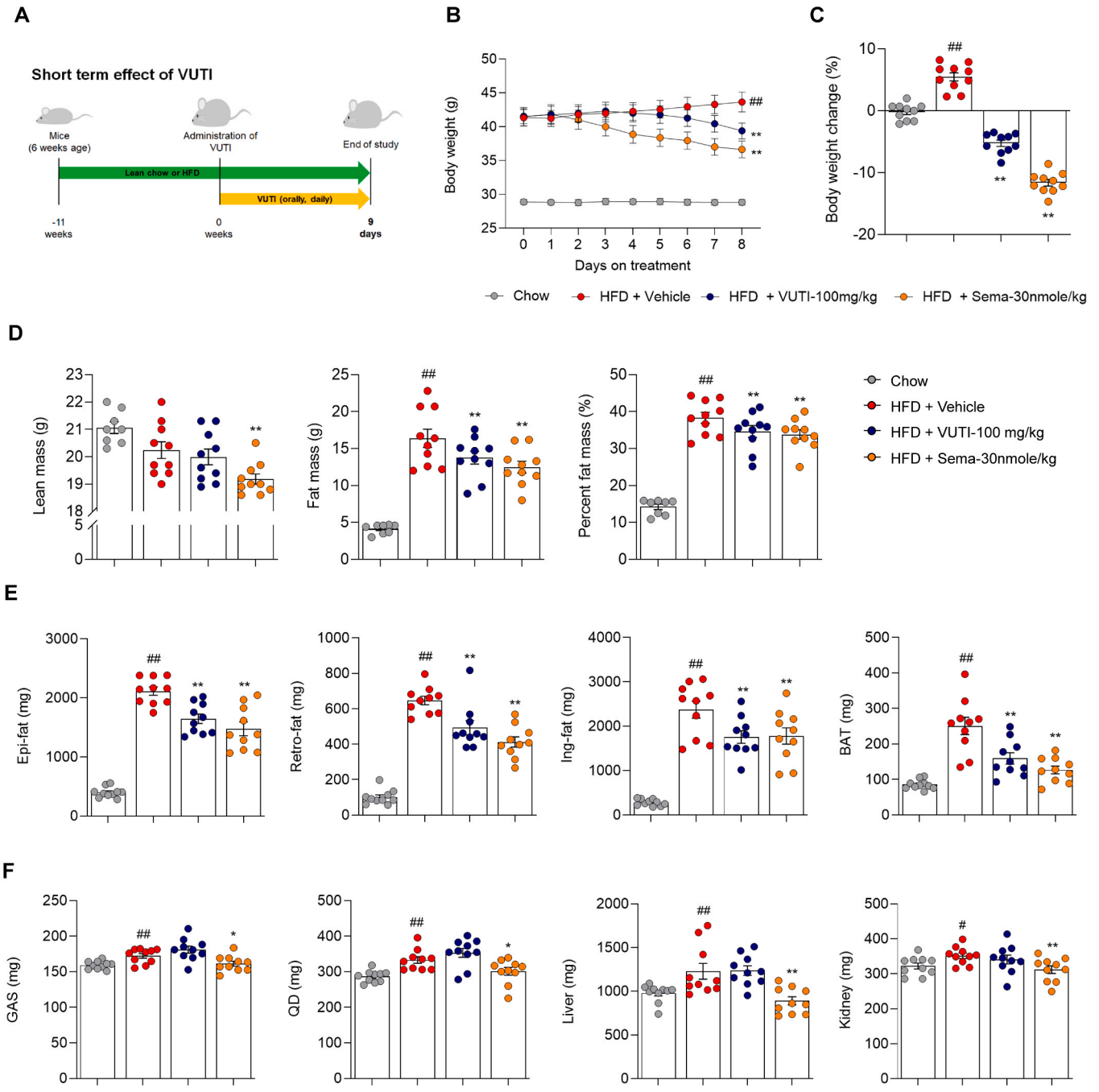


**Fig. 2.** Short-term Effect of Vutiglabridin (VUTI) and Semaglutide (Sema) in high-fat diet (HFD)-induced obese mice. Mice were fed an HFD for 11 weeks and administered VUTI or Semaglutide (Sema) once daily for 9 days. (A) Schematic diagram of experiment study design; (B) Daily body weight change; (C) Relative weight change; (D) Dual X-ray absorptiometry (DXA) analysis; (E) Fat tissues weight; (F) Peripheral tissues weight. Data are presented as mean ± SEM (n = 10 for each group). Groups with different letters statistically differ (for the HFD group compared to the lean group: # $p < 0.05$, ## $p < 0.01$; for the VUTI and Sema group compared to the HFD group: * $p < 0.05$, ** $p < 0.01$). P-value was assessed by one-way ANOVA with Tukey's multiple comparison test. Epi-fat, epididymal fat; Retro-fat, retro-peritoneal fat; Ing-fat, Inguinal-fat; BAT, interscapular brown adipose tissues; GAS, gastrocnemius muscle; QD, quadriceps muscle.

D). VUTI dose-dependently reduced adipose tissue weights and plasma leptin, and mice treated with VUTI 100 mg/kg exhibited adipose tissue weights similar to those of lean controls (Fig. 3E and S2B). While no muscle mass loss was observed in the 50 mg/kg group, a modest reduction in muscle weight (GAS and QD) was noted in the 100 mg/kg group, likely attributable to a transient decrease in food intake during long-term treatment (Fig. 3F and S3A). Adipose tissue macrophages are infiltrated surround dead and inflamed adipocytes, forming so-called crown-like structures (CLS) [31]. Immunohistochemical data for F4/80 staining revealed that VUTI treatment significantly reduced the levels of adipose tissue macrophages and adipocyte size compared to untreated HFD groups (Fig. 3G and H). In both short-term (9-day) and long-term (6-week) treatment models, VUTI and Sema significantly reduced plasma lipid levels, including total cholesterol, HDL-cholesterol, and LDL-cholesterol, and improved glucose homeostasis, as evidenced by reductions in plasma glucose and insulin levels (Fig. S2A and S2B). To further investigate the effects of VUTI on energy homeostasis, including energy expenditure, energy absorption, and fecal energy excretion, we conducted a comprehensive metabolic analysis using the CLAMS system [25]. VUTI treatment led to a dose-dependent

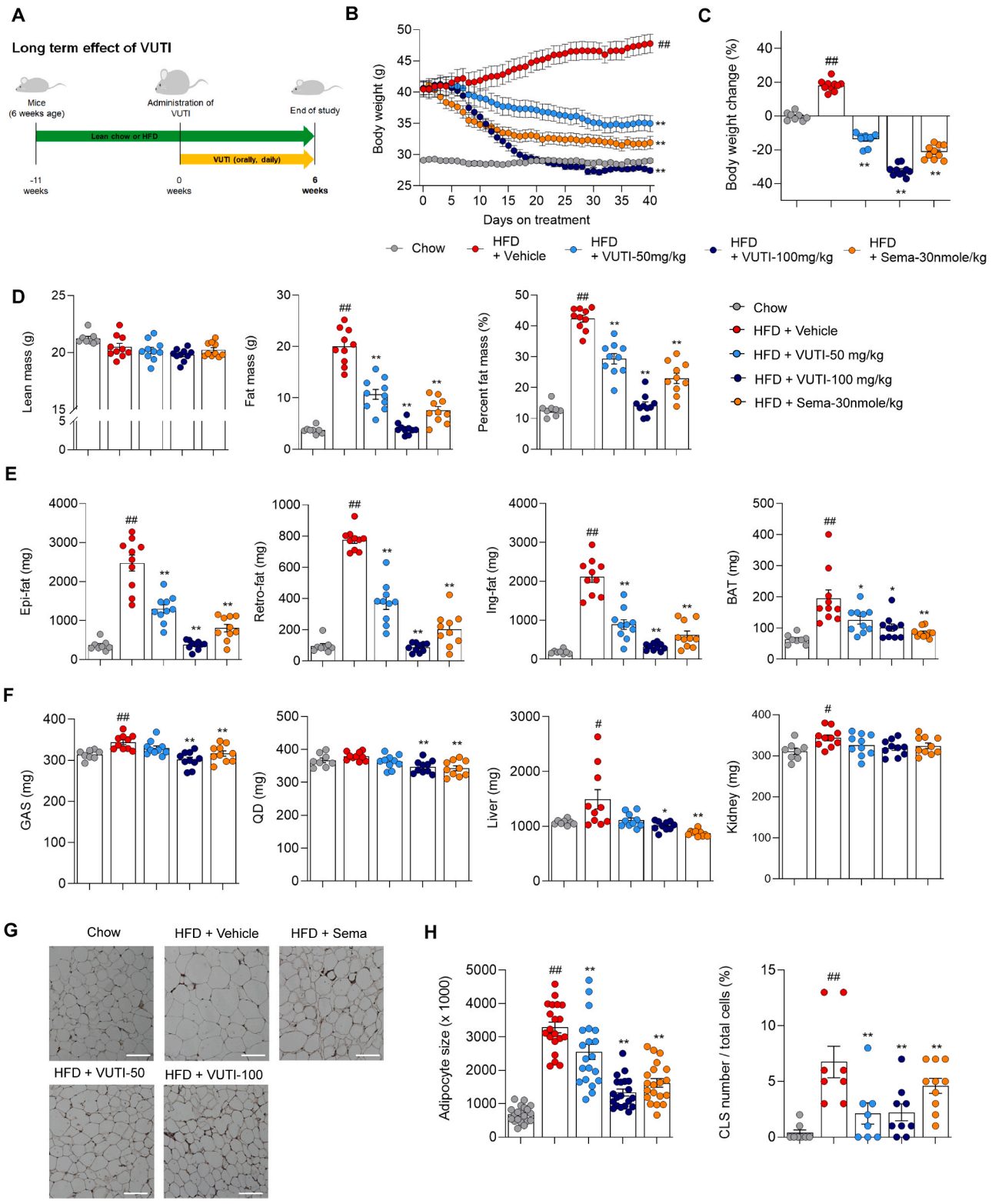


**Fig. 3.** Long-term effect of Vutiglabridin (VUTI) and Semaglutide (Sema) in high-fat diet (HFD)-induced obese mice. Mice were fed an HFD for 11 weeks and administered VUTI or Semaglutide (Sema) once daily for 6 weeks. (A) Schematic diagram of experiment study design; (B) Daily body weight change; (C) Relative weight change; (D) Dual X-ray absorptiometry (DXA) analysis; (E) Fat tissues weight; (F) Peripheral tissues weight; (G) Representative F4/80 stained images in epididymal fat (scale bar = 10 μm); (H) Quantification of adipocyte size and crown-like structure in epididymal fat. Data are presented as mean ± SEM (n = 8 for the lean group; n = 10 for the HFD group; n = 10 for the 50 or 100 mg/kg VUTI-treated group; n = 10 for the Sema-treated group). Groups with different letters statistically differ (for the HFD group compared to the lean group: # $p < 0.05$, ## $p < 0.01$; for the VUTI and Sema group compared to the HFD group: * $p < 0.05$, ** $p < 0.01$). P-value was assessed by one-way ANOVA with Tukey's multiple comparison test. Epi-fat, epididymal fat; Retro-fat, retro-peritoneal fat; Ing-fat, Inguinal-fat; BAT, interscapular brown adipose tissues; GAS, gastrocnemius muscle; QD, quadriceps muscle.

increase in oxygen consumption ($VO_2$), carbon dioxide production ($VCO_2$), total energy expenditure, and locomotor activity (Fig. S3B–E). However, no significant changes were observed in energy absorption or fecal energy excretion following VUTI treatment (Fig. S3F and S3G). Overall, these results suggest that VUTI not only reduces fat but also exerts beneficial effects on overall metabolic improvement.

### 3.4. VUTI inhibits adipogenesis in adipocytes

To investigate the mechanism of VUTI, we assessed its effect on adipogenesis. 3T3-L1 murine preadipocytes were differentiated with MDI treatment for 8 days with or without of VUTI (Fig. 4A). MDI treatment markedly increased both total lipid and TAG levels in adipocytes, whereas co-treatment with VUTI significantly suppressed MDI-induced lipid and TAG accumulation (Fig. 4B, C, and D). During adipocyte differentiation, intracellular reactive oxygen species (ROS) act as signaling mediators that activate adipogenic transcription factors, including PPARγ, C/EBPα, and SREBP1c [32–34]. Thus, we evaluated whether VUTI modulates ROS levels during adipocyte differentiation. Both ROS generation and lipid peroxidation were elevated during the differentiation of preadipocytes, whereas their accumulations were markedly reduced by VUTI treatment (Fig. 4E and F). Consistently, VUTI also suppressed adipogenesis in human white preadipocytes in differentiation media for 15 days, as evidenced by Oil red O staining (Fig. 4G–I). These findings indicate that VUTI inhibits adipogenesis in both murine and human adipocytes, at least in part, by reducing ROS levels during the differentiation.

### 3.5. VUTI decreases lipid accumulation in mature adipocytes

To investigate the lipid-degradation effects of VUTI in mature adipocytes, differentiated 3T3-L1 murine adipocytes were treated with VUTI for 1 day to assess short-term effects and for 5 days to assess long-term effects. (Fig. 5A and S4A). Compared to untreated controls, VUTI treatment significantly reduced total lipid and intracellular TAG levels (Fig. 5B–D). TAG hydrolysis is primarily regulated by two key lipases: ATGL, which initiates TAG breakdown, and HSL, which catalyzes the conversion of diacylglycerol (DAG) to monoacylglycerol (MAG) [35,36]. Because HSL activity is regulated by its phosphorylation status, we examined ATGL expression and HSL phosphorylation. Interestingly, VUTI increased ATGL expression while reducing HSL phosphorylation (Fig. 5D and S4B), suggesting that VUTI promotes ATGL-mediated lipolysis independently of HSL activation. Consistent with enhanced lipolysis, glycerol release was significantly elevated in VUTI-treated adipocytes compared to untreated controls (Fig. 5E). In addition, VUTI increased the expression of ATGL, a key enzyme involved in basal lipolysis, while reducing the level of phosphorylated HSL, which is typically activated by the β-adrenergic receptor PKA signaling axis

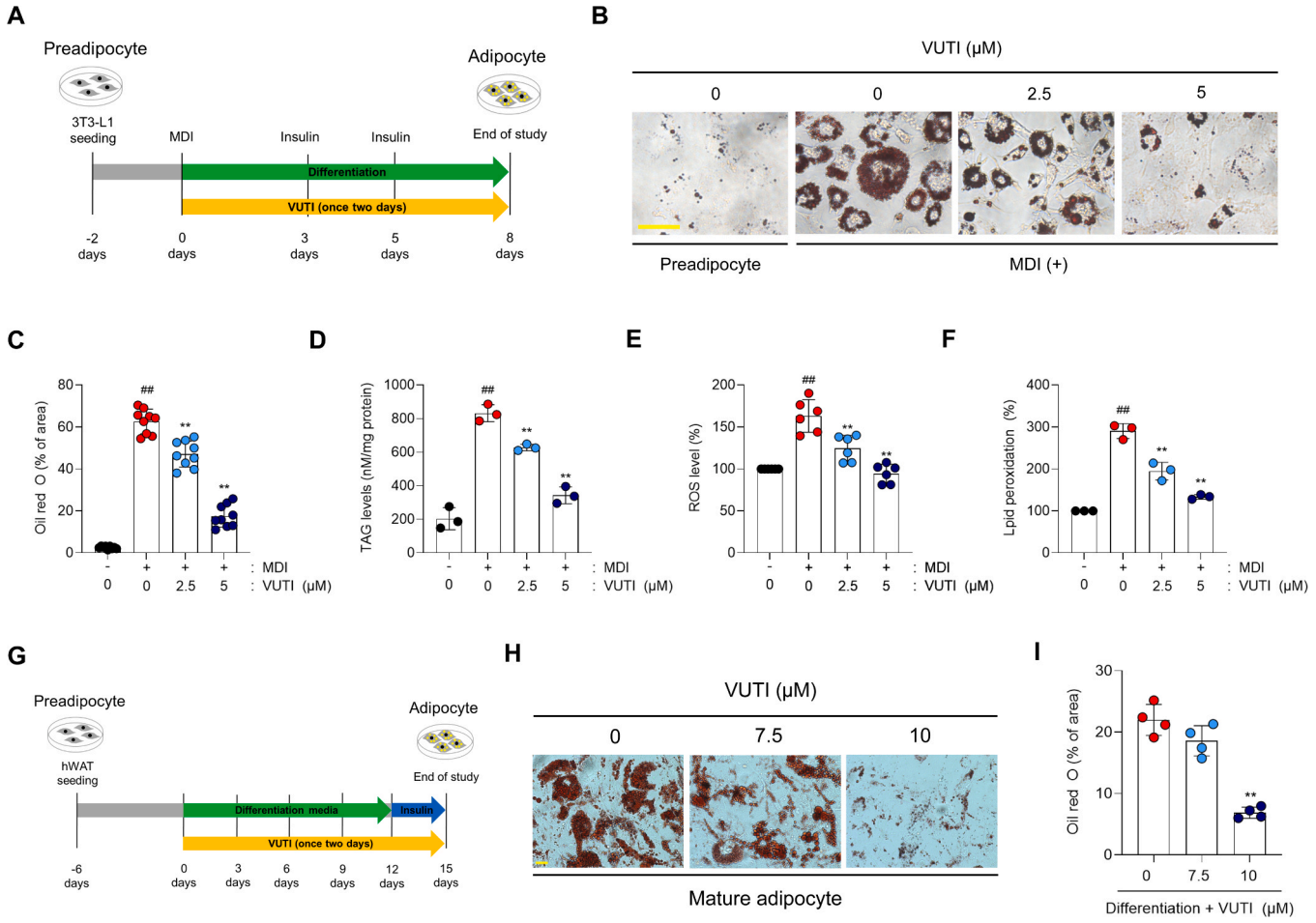


**Fig. 4.** Effect of VUTI on adipogenesis in 3T3-L1 murine adipocytes and human white adipocytes. (A) Schematic diagram for effect of VUTI on adipogenesis in 3T3-L1 murine preadipocytes; (B) Representative Oil red O (ORO)-stained images (scale bar = 10 μm); (C) Quantitative analysis of ORO-stained cells (n = 9); (D) triacylglycerol (TAG) levels (n = 3); (E) ROS level (n = 4); (F) Lipid peroxidation (n = 3). (G) Schematic diagram for effect of VUTI on adipogenesis in human white preadipocytes; (H) Representative Oil red O (ORO)-stained images (scale bar = 20 μm); (I) Quantitative analysis of ORO-stained cells (n = 4). Data are presented as mean ± standard deviation. Groups with different letters statistically differ (for the mature adipocytes compared to the preadipocytes: # $p < 0.05$, ## $p < 0.01$; for the VUTI-treated group compared to the control group: * $p < 0.05$, ** $p < 0.01$). p value was assessed by two-trailed Student's *t*-test.

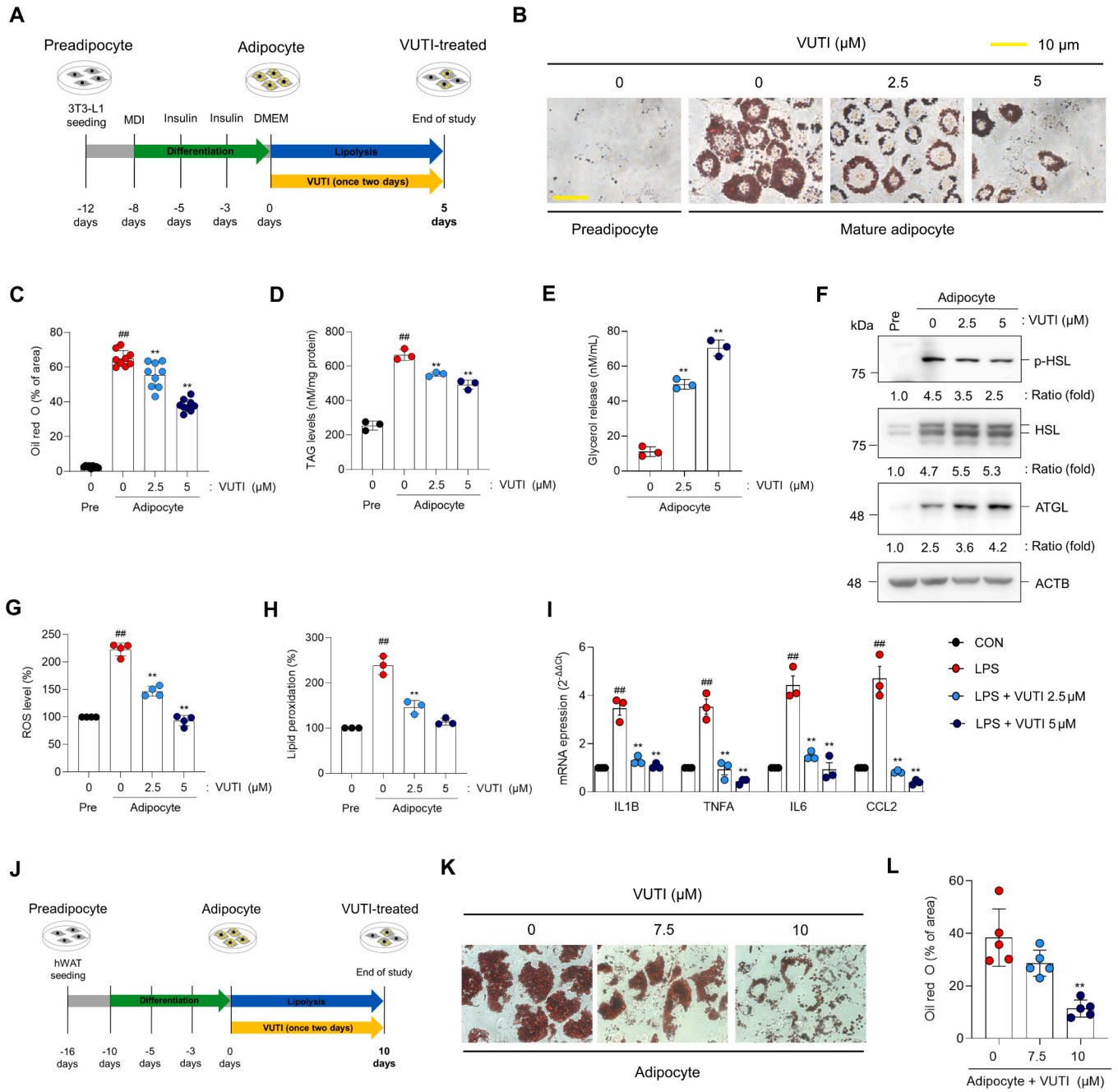


**Fig. 5.** Effect of VUTI on lipolysis in 3T3-L1 murine adipocytes and human white adipocytes. (A) Schematic diagram for effect of VUTI on lipolysis in 3T3-L1 murine adipocytes; (B) Representative Oil red O (ORO)-stained images (scale bar = 10 μm); (C) Quantitative analysis of ORO-stained cells (n = 9); (D) triacylglycerol (TAG) levels (n = 3); (E) Release of glycerol (n = 3); (F) Immunoblot analysis of lipase activity (phosphorylation of HSL and expression of ATGL); (G) ROS level (n = 4); (H) Lipid peroxidation (n = 3); qPCR analysis of inflammatory genes (IL1B, TNF, IL6, and CCL2) in LPS-stimulated adipocytes with or without VUTI, normalized by ACTB (n = 3). (J) Schematic diagram for effect of VUTI on lipolysis in human white adipocytes; (K) Representative ORO-stained images (scale bar = 20 μm); (L) Quantitative analysis of ORO-stained cells (n = 4). DATA are presented as mean ± standard deviation. Groups with different letters statistically differ (for the mature adipocytes compared to the preadipocytes: ## $p < 0.01$; for the VUTI-treated group compared to the control group: ** $p < 0.01$). p value was assessed by two-trailed Student's *t*-test.

(Fig. 5F). VUTI treatment significantly decreased intracellular ROS levels and lipid peroxidation in mature adipocytes (Fig. 5G and H). Excessive lipid accumulation is closely associated with adipose tissue inflammation (Fig. 3G) [37,38]. Since inflamed adipocytes exhibit elevated oxidative stress and impaired lipid metabolism, including dysregulated lipolysis [39,40], we next investigated the effects of VUTI on inflammatory responses under lipopolysaccharide (LPS) induced inflammatory conditions [41]. LPS stimulation markedly increased the expression of inflammatory mediators such as IL1B, TNFA, IL6, and CCL2. Notably, co-treatment with VUTI significantly suppressed the expression of these pro-inflammatory genes, restoring their levels to near those of the control group (Fig. 5I). VUTI also suppressed lipid accumulation in differentiated human white adipocytes following 10 days of treatment, as confirmed by Oil red O staining (Fig. 5J–L). These results indicate that VUTI not only reduces lipid accumulation but also effectively attenuates oxidative stress and inflammation in adipocytes.

### 3.6. VUTI decreases lipid accumulation in a PON2-dependent manner

VUTI has previously been reported to directly bind to paraoxonase 2 (PON2), restoring its enzymatic activity under lipotoxic conditions in L-02 hepatocytes, thereby activating autophagy and mitophagy and suppressing lipid accumulation [30,42]. In this study, VUTI increased both the lactonase and esterase activities of PON2 in mature human white adipocytes and 3T3-L1 murine adipocytes (Fig. 6A). However, VUTI did not affect PON2 expression levels (Fig. 6B). To determine whether PON2 activation is required for the lipid degradation of VUTI, mature adipocytes were treated with VUTI under PON2 knockdown (KD) conditions. In control adipocytes, VUTI suppressed lipid accumulation in a dose-dependent manner. However, in PON2 KD adipocytes, VUTI induced lipid degradation was completely abolished, demonstrating that this effect is mediated by PON2 activation (Fig. 6C and D). Next, we examined whether VUTI-induced autophagy activation is also dependent on PON2. Immunoblot analysis showed that the autophagic flux marker SQSTM1 was degraded following VUTI treatment in control adipocytes, whereas it remained unchanged in PON2 KD adipocytes (Fig. 6E). Furthermore, VUTI upregulated the expression of autophagosome formation-associated proteins, including BECN1 and ATG3, in mature adipocytes, while no such increase was observed in the PON2 KD adipocytes (Fig. 6E). The reduction in lipid accumulation induced by VUTI in adipocytes was observed without affecting cell viability (Fig S5A and S5B). Collectively, these findings indicate that VUTI suppresses lipid accumulation and activates autophagy in adipocytes through PON2-dependent mechanisms.

### 3.7. AMPK activation is keystone for VUTI-induced lipophagy in adipocytes

Similar to the effect of VUTI on PON2 activity and expression in mature human white adipocytes (Fig. 6A and B), VUTI also increased PON2 activity in 3T3-L1 murine adipocytes without changing its expression (Fig. 7A and B).

VUTI promotes the degradation of intracellular lipid droplets (LDs) and TAG in mature adipocytes; however, HSL-dependent lipolysis, which catalyzes the conversion of DAG to MAG, was incompletely

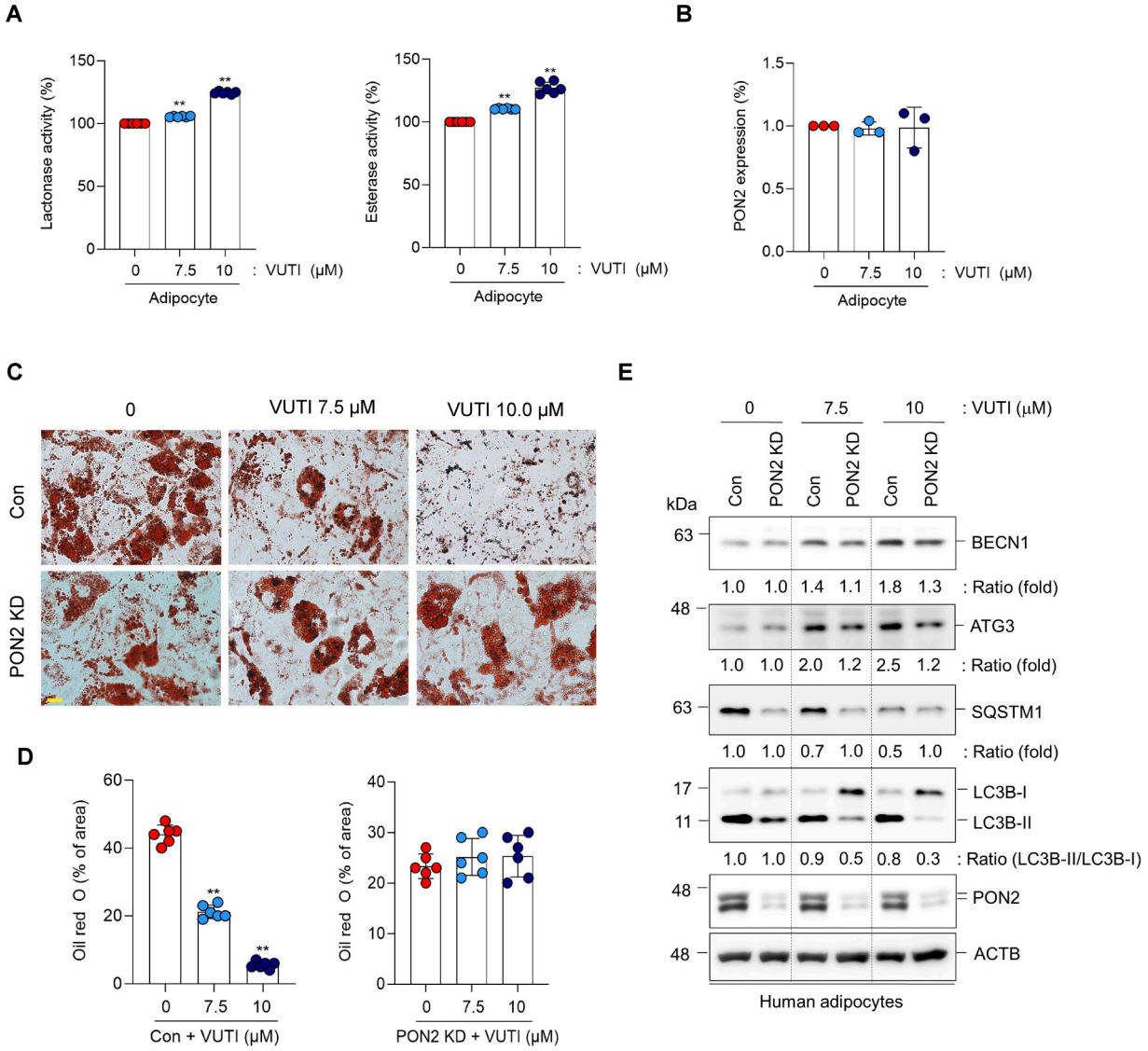


**Fig. 6.** Effect of VUTI on PON2-dependent lipolysis. (A) PON2 activity in mature human white adipocytes after 10-day VUTI treatment; (B) PON2 expression in adipocytes is shown in (A). (C) Representative Oil red O (ORO)-stained images (scale bar = 20 μm) in PON2 KD and control human white adipocytes; (D) Quantitative analysis of ORO-stained PON2 KD and control cells (n = 6). (E) Immunoblot analysis of autophagy activation in mature human white adipocytes after 10-day treatment with VUTI, normalized by ACTB. Data are presented as mean ± standard deviation. Groups with different letters statistically differ (for the VUTI-treated group compared to the control group: ** $p < 0.01$). P-value was assessed by two-trailed Student's *t*-test.

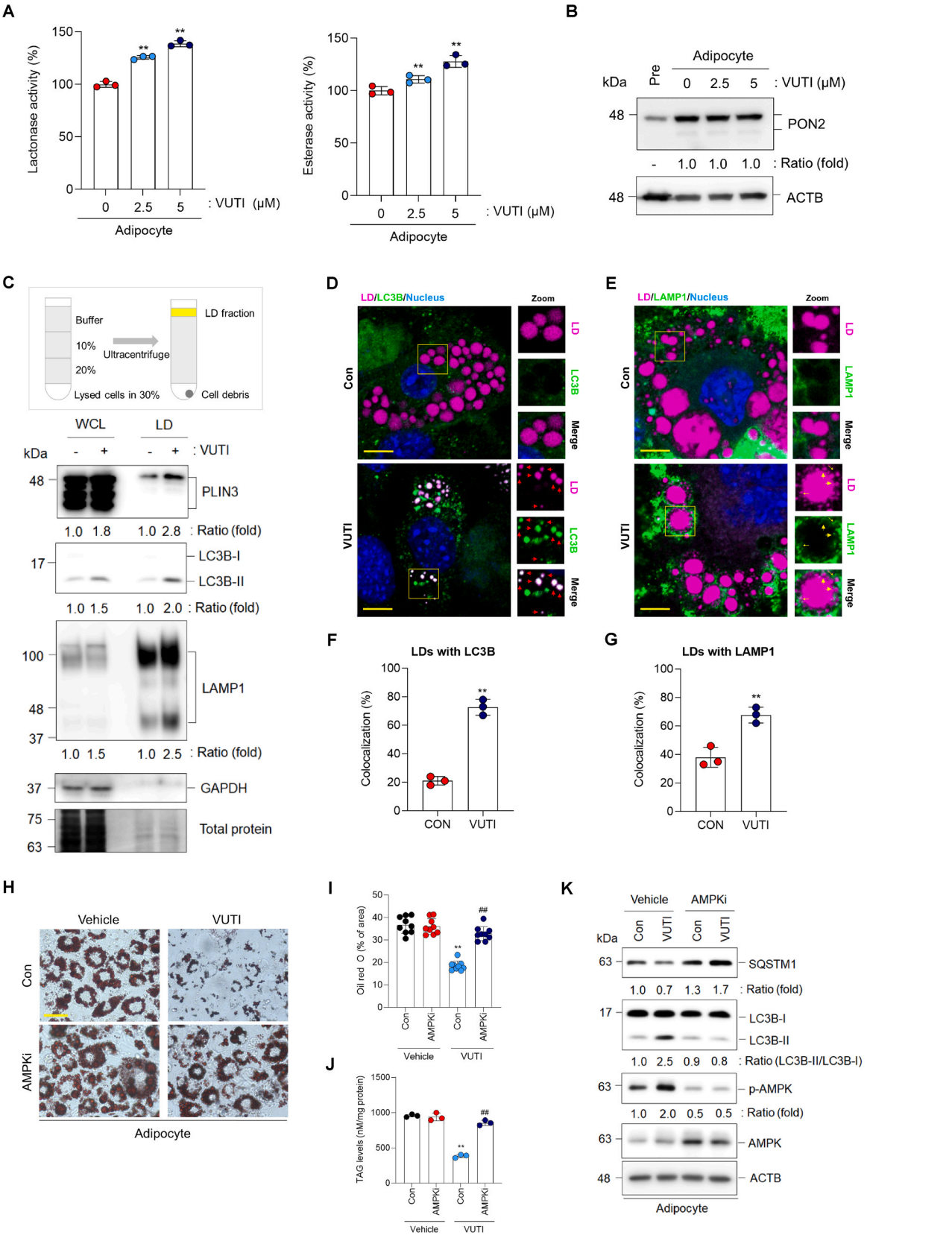


*(caption on next page)*

**Fig. 7.** Effect of VUTI on AMPK-mediated lipophagy in adipocytes. (A) PON2 activity in mature 3T3-L1 murine adipocytes after 5-day VUTI treatment; (B) PON2 expression in adipocytes is shown in (A). Analysis of the contents of lipophagy markers in lipid droplet (LD) from VUTI- and control-treated adipocytes. (C) Schematic diagram of experimental study for LDs fractionation in adipocytes is shown in upper panel. Immunoblot data for determining the contents of lipophagy markers in the fractionated LDs and whole cell lysates. All bands from whole cell lysates are normalized by GAPDH, as a negative marker for fractionated LD. Total protein is shown as a loading control in fractionated LDs. (D-E) Confocal analysis of the effect of VUTI on distribution of autophagy (LC3B) and lysosome (LAMP1) in Lipid droplets (LDs); (F-G) Quantitative analysis of the effect of VUTI on colocalization of autophagy and lysosome in LDs (n = 3). Mature adipocytes are treated with VUTI alone or combined with VUTI and AMPK inhibitor for 5 days. (H) Representative ORO-stained images (scale bar = 10 μm); (I) Quantitative analysis of ORO-stained cells (n = 9); (J) Quantitative analysis of TAG level (n = 3); (K) Immunoblot analysis of AMPK and autophagy markers, all bands are normalized by ACTB. Data are presented as mean ± standard deviation. Groups with different letters statistically differ (for the VUTI-treated group compared to the control group: ** $p < 0.01$; for the VUTI-treated adipocytes compared to the AMPKi vehicle: ## $p < 0.01$). P-value was assessed by two-trailed Student's *t*-test.

activated by VUTI. Since autophagic degradation of intracellular LDs (especially termed as lipophagy) represents another key mechanism contributing to lipolysis in adipocytes [43,44], we next investigated whether VUTI promotes lipid degradation through lipophagy activation in mature 3T3-L1 adipocytes. Immunoblot analysis revealed that the autophagic flux marker SQSTM1 was accumulated in mature adipocytes compared to preadipocytes, whereas it was degraded following VUTI treatment (Fig. S6A). In addition, the expression of autophagosome-associated proteins including BECN1, ATG3, and the LC3B-II/LC3B-I ratio was suppressed in mature adipocytes but significantly increased upon VUTI treatment (Fig. S6A), further supporting the reactivation of autophagy by VUTI. We next assessed lipophagy activation by performing biochemical fractionation of LD from VUTI-treated mature adipocytes. LD fraction analysis revealed that VUTI treatment increases the LD localization of lipophagy-related proteins including PLIN3, LC3B-II, and LAMP1 in mature adipocytes (Fig. 7C). Consistent with this result, confocal microscopy analysis showed that VUTI treatment reduced both the size and number of LDs, and increased the number of LDs colocalized with LC3B (Fig. 7D and F). Furthermore, VUTI treatment also increased the number of LDs colocalized with LAMP1 (Fig. 7E and G), showing that VUTI treatment increases the formation of small LDs engulfed by lysosomes.

AMPK is a key metabolic regulator that promotes lipid degradation through increase of ATGL expression and induction of autophagy via phosphorylation of autophagy-related kinases and transcription factors [45–47]. To investigate whether VUTI-induced lipophagy is mediated by AMPK, we assessed AMPK activation in mature adipocytes. Immunoblotting showed that AMPK phosphorylation was significantly reduced in mature adipocytes relative to preadipocytes; VUTI treatment restored p-AMPK levels (Fig. S6B). The AMP/ATP ratio, which reflects the cellular energy level, indirectly regulates AMPK activity [48]. VUTI treatment increased AMP levels and decreased ATP levels, resulting in a significantly elevated AMP/ATP ratio (Fig. S6C), indicating induction of energy stress and subsequent AMPK activation. To determine whether AMPK activation is required for VUTI-induced autophagy, mature adipocytes were treated with VUTI with or without Compound C, a pharmacological AMPK inhibitor. Inhibition of AMPK also suppressed VUTI-induced LD degradation and TAG hydrolysis (Fig. 7H–J), and abolished the VUTI-induced increase in autophagy, suggesting that AMPK plays a critical role in mediating the lipid degradation of VUTI.

To validate the mechanism of VUTI action in adipose tissue, we analyzed epididymal white adipose tissue from DIO-mice treated with VUTI or Sema for 9 days using transcriptomic, proteomic, and immunoblot analyses (Fig. 8A). Among 8506 identified proteins, differentially expressed proteins (DEPs) were determined by comparing VUTI or Sema-treated groups with the DIO-vehicle group (Fig. 8B). Compared with the vehicle group, 482 proteins were significantly upregulated in the VUTI group, of which 332 were uniquely increased in VUTI without overlapping with Sema. Conversely, of the 390 proteins significantly downregulated in the VUTI group, 213 were uniquely decreased in VUTI without overlapping with Sema (Fig. 8C). Functional annotation revealed that VUTI-specific DEPs were enriched in processes related to lipase activity, antioxidant activity, and autophagy, while processes associated with immune response and ATP activity were specifically decreased. Notably, VUTI uniquely increased proteins involved in AMPK signaling (Adipoq, Foxo1), autophagy (Becn1, Map1lc3b), and lipolysis (Abhd5, Pnpla2, Lipe), whereas lipogenesis-related proteins (Gpam, Mogat2) were commonly decreased in both VUTI and Sema-treated groups (Fig. 8D). At the mRNA level, a similar pattern was observed: VUTI uniquely upregulated AMPK related genes (Creb3l2, Pik3r2, Ppargc1a) and autophagy related genes (Atg4a, Ambra1, Hdac6), while lipogenesis related genes (Acaca, Fasn, Dgat2, Srebf1) were commonly downregulated by both VUTI and Sema (Fig. 8E). In immunoblot analysis, we confirmed that the reduced Prkaa2 (AMPK) expression and phosphorylation observed in DIO-mice compared with lean controls were restored by VUTI, thereby promoting autophagy activation, as evidenced by increased levels of ATG3 and BECN1 (Fig. 8 F, G, and S7). Consistent with AMPK phosphorylation, PON2 activity was also diminished in DIO-mice compared with lean controls, and VUTI restored PON2 activity without altering PON2 expression (Fig. 8H and I).

Overall, these findings suggest that suppression of PON2 activity and AMPK signaling in adipose tissue contributes to lipid accumulation in adipocytes. VUTI restores PON2 activity, thereby promoting AMPK-mediated lipid degradation in adipocytes and leading to fat-selective reduction.

## 4. Discussion

Adipose tissue plays a central role in regulating whole-body energy homeostasis. Dysregulation of adipocyte lipid metabolism leads to excessive fat deposition and the development of obesity. Recently, emerging evidence has indicated that, in addition to increased lipogenesis driven by excessive caloric intake, the impaired lipid catabolic process in adipose tissue also plays a critical role in exacerbating fat accumulation [11–14]. Therefore, effective obesity treatment requires not only appropriate caloric restriction but also restoration of defective lipolysis in adipose tissue. Our study provides that VUTI exerts significant reductions in body weight and fat mass in DIO mice by increasing PON2 activity, thereby activating autophagy in adipose tissue. Additionally, VUTI directly suppresses adipogenesis and promotes autophagy-driven lipid degradation in both 3T3-L1 murine adipocytes and human adipocytes.

Leo et al. reported that VUTI induces dose-dependent body weight loss and exhibits superior anti-obesity effects compared to pair-fed group in HFD mice [22]. Notably, in the high-dose group (100 mg/kg), VUTI markedly reduced adipose tissue mass (epididymal and perirenal adipose tissues), as well as adipocyte size, to levels comparable to those of lean control mice. Alongside reductions in body weight and fat mass, key metabolic parameters including circulating glucose, insulin, and leptin were also significantly improved. Using the Comprehensive Laboratory Animal Monitoring System (CLAMS) [25], VUTI was shown to increase energy expenditure, accompanied by upregulated expression of metabolic genes such as Pgc-1α, Prkaa2, and Foxo1 in muscle and liver tissues. These findings indicate that VUTI enhances whole-body energy metabolism and contributes to its anti-obesity effects in DIO-mice. In addition, VUTI ameliorated hepatic steatosis and reduced liver injury markers, accompanied by a reduction in body weight, in several metabolic dysfunction-associated steatohepatitis mouse models [30]. Unlike previous studies, we examined the tissue distribution of VUTI to investigate its fat-reducing effects. Our

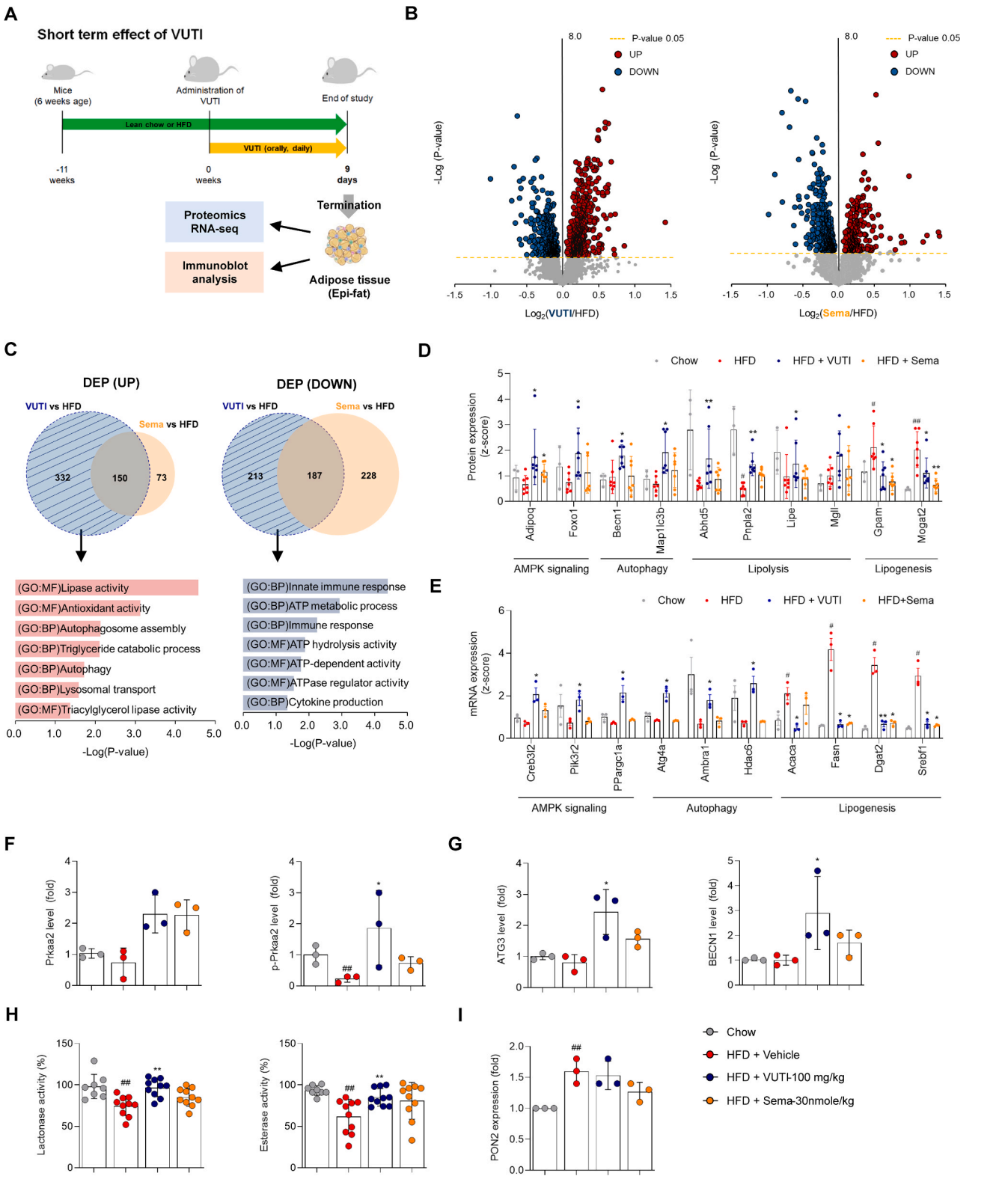


**Fig. 8.** Effect of VUTI on white adipose tissue in HF-DIO. Mice were administered VUTI or Semaglutide (Sema) once daily for 9 days, followed by proteomic, transcriptomic, and immunoblot analyses of white adipose tissue (WAT). (A) Schematic diagram of experiment study design. Proteomic analysis in WAT from chow-fed (n = 3) and HF-DIO mice treated with vehicle (n = 7), VUTI (n = 7), and Sema (n = 7). (B) Volcano plot analysis; (C) Venn diagram of differentially expressed proteins (DEPs) between the VUTI/Sema and vehicle groups, and gene ontology (GO) analysis of VUTI-specific DEPs; (D) AMPK signaling, autophagy, lipolysis, and lipogenesis-related DEPs; (F) AMPK signaling, autophagy, and lipogenesis-related DEGs. Transcriptomic analysis, PON2 enzyme activity, immunoblot analysis of p-AMPK levels, and autophagy activation in WAT from lean (n = 3) and HF-DIO mice treated with chow-fed (n = 3), VUTI (n = 3), or Sema (n = 3). (F) Prkaa2 and p-Prkaa2 activation; (G) ATG3 and BECN1 activation. DATA are presented as mean ± standard deviation. (H) PON2 enzyme activity (esterase and lactonase activity); (I) Pon2 expression; Groups with different letters statistically differ (for the HFD group compared to the lean group: # $p < 0.05$, ## $p < 0.01$; for the VUTI and Sema group compared to the HFD group: * $p < 0.05$, ** $p < 0.01$). P-value was assessed by two-trailed Student's *t*-test.

results demonstrate that VUTI preferentially distributes to adipose tissues, with more than 10-fold higher exposure in adipose tissues compared to the plasma (Fig. 1B). These findings strongly suggest that adipose tissue is a primary pharmacological target of VUTI. In particular, VUTI exhibits a distinct pattern of weight loss compared to Sema, whose primary mechanism of action is appetite suppression. In the short-term (9-day) treatment study using DIO-mice, Sema induced rapid body weight loss within the first few days, whereas VUTI resulted in minimal weight change during the initial 4 days (Fig. 2B and C). By day 9, Sema reduced both lean and fat mass, while VUTI selectively decreased fat mass while preserving lean mass, including skeletal muscle (Fig. 2D–F). At 100 mg/kg, VUTI reduced body weight and fat mass to levels comparable to those of lean mice within 3 weeks, and also significantly decreased liver mass (Fig. 3B, D–F). Following this period, no decrease in food intake was observed, and body weight remained stable without further reduction (Fig 3B, S3A). Throughout the 6-week treatment period, no adverse events or behavioral abnormalities were observed in any animals treated with VUTI at 100 mg/kg (data not shown). Moreover, in the CLAMS study conducted after 4 weeks of dosing, when body weight had reached the lean range, VUTI-treated mice showed increased energy expenditure and physical activity, reflecting an improvement in overall metabolic health (Fig S3B–E). To elucidate the mechanism of VUTI, we conducted in *vitro* studies and demonstrated that VUTI directly suppresses adipogenesis and promotes lipid degradation via lipophagy in adipocytes. Additionally, we confirmed that VUTI-induced lipid degradation in adipocytes occurs through PON2, a known target of VUTI. This finding provides the first evidence identifying PON2 as a key regulator of lipid metabolism in adipocytes.

In *in vivo* PON2-knockdown mice fed a high-fat diet, body weight increased significantly compared to wild-type controls, primarily due to a selective gain in fat mass, while lean mass remained largely unchanged [49]. Although PON2 is considered to play an important role in adipose tissue, its specific role in adipocyte lipid metabolism has not yet been elucidated. PON2 is a multifunctional enzyme known for its potent antioxidant properties, particularly in mitigating mitochondrial ROS and cellular oxidative stress [50,51]. ROS have been shown to play an essential role in the regulation of adipogenesis. Transient increases in intracellular ROS levels are required for the initiation and progression of adipocyte differentiation, functioning as signaling molecules that promote the expression of adipogenic transcription factors such as PPARγ and C/EBPα [32–34]. Accordingly, treatment with antioxidants including N-acetylcysteine during adipocyte differentiation has been shown to reduce cellular ROS level and inhibit adipogenesis [52]. In this study, we demonstrated that VUTI, a pharmacological activator of PON2, effectively reduced intracellular ROS levels in adipocytes in a dose-dependent manner (Fig. 4E). Concurrently, VUTI suppressed the differentiation of preadipocytes into mature adipocytes under adipogenic conditions (Fig. 4B and C). These results suggest that the activation of PON2 in adipocytes attenuates ROS accumulation and, in turn, inhibits adipogenesis, further supporting its role as a key regulator of adipocyte differentiation.

The function of PON2 in adipocyte lipid degradation has yet to be clearly elucidated, and it is difficult to attribute the lipid degradation in adipocytes solely by its ROS-reducing effect. Shin et al. previously reported that, in hepatocytes, PON2 plays a distinct role in regulating autophagy [30,42]. In PON2-knockdown L-02 hepatocytes, autophagic flux was suppressed, leading to reduced mitophagy, ultimately impairing mitochondrial function. These findings indicate that PON2 acts as a regulator of autophagy. In this study, we demonstrated that PON2 activation in adipocytes also induces autophagy that specifically targets LDs through the lysosomal degradation pathway, a process known as lipophagy. VUTI increased PON2 activity and promoted lipid degradation in both 3T3-L1 murine adipocytes and human adipocytes in a dose-dependent manner (Figs. 6A and 7A). Mechanistically, VUTI increased the protein expression of autophagosome formation markers including LC3B, ATG3, and BECN1 while decreasing the expression of the autophagic substrate SQSTM1 (Fig. S4B). Moreover, analysis of isolated LDs revealed that VUTI upregulated the expression of lipophagy markers such as PLIN3 and LAMP1, providing direct evidence that VUTI induces lipid degradation via lipophagy (Fig. 7C). Another notable finding is that VUTI promotes PON2 activation and AMPK-mediated lipolysis, leading to lipid degradation. In 3T3-L1 adipocytes, VUTI treatment increased the expression of ATGL, a key enzyme involved in basal lipolysis, while reducing the level of HSL, which is a major regulator of hormone-stimulated lipolysis (Figs. 5F and 8D).

AMPK is a key regulator of energy metabolism across multiple tissues. Under conditions of energy stress, AMPK phosphorylation promotes autophagy to remove damaged cellular components and enhances mitochondrial biogenesis to maintain cellular homeostasis [48,53]. Recent studies have revealed that, in adipocytes, AMPK acts as a key regulator of lipid metabolism and its activation suppresses lipogenesis [54]. In our *in vivo* experiments, obese mice exhibited decreased PON2 activity and p-AMPK levels, accompanied by increased expression of lipogenesis-related genes (Acaca, Fasn, Dgat2, and Srebf1) in adipose tissue compared with lean controls (Fig. 8E, F, H). We demonstrated that VUTI treatment decreases the expression of lipogenesis-related genes at both the mRNA (Acaca, Fasn, Dgat2, and Srebf1) and protein levels (Gpam and Mogat2) (Figs. 8D and 8E). These findings suggest that the inhibition of lipid synthesis by VUTI is a consequence of AMPK activation and contributes to its fat-reducing effects. Activation of AMPK not only suppresses lipogenesis but also promotes lipolysis through a non-canonical pathway distinct from PKA-mediated canonical lipolysis by regulating lipase activity via ATGL [45,47,55,56].

In DIO-mice adipose tissue, lipase expression was also decreased, with a particularly significant reduction in the expression of ATGL, which is encoded by the *Pnpla2* gene (Fig. 8D). VUTI restored ATGL and ABHD5 expression in adipose tissue and activated autophagy (Fig. 8D and G). These findings suggest that impaired AMPK signaling in adipose tissue may be a key contributor to fat accumulation and the development of obesity. Furthermore, activation of PON2 represents a potential therapeutic strategy for improving obesity by restoring impaired p-AMPK, thereby promoting fat reduction.

The first strength of this study is the demonstration that improving p-AMPK–mediated lipid metabolism in adipose tissue can be an effective strategy to ameliorate obesity. In DIO mice, both p-AMPK and lipase activity, particularly that of ATGL, were reduced. VUTI restored levels of p-AMPK and ATGL, resulting in a fat-selective weight loss effect. Second, we identified PON2 in adipose tissue as a novel therapeutic target for obesity treatment. Activation of PON2 in adipocytes not only suppressed adipogenesis but also promoted lipid degradation. However, several limitations remain. Although our data indirectly support a link between PON2 activation and AMPK signaling, the precise molecular mechanism by which PON2 regulates AMPK activity has yet to be elucidated. Further studies are needed to clarify the relationship between PON2 function and AMPK activation.

In conclusion, our study demonstrates that VUTI preferentially distribute in adipose tissue and promotes AMPK/lipophagy through PON2 activation, resulting in significant reductions in body weight and fat mass in obese mice. Furthermore, our findings in both 3T3-L1 murine adipocytes and human adipocytes show that VUTI suppresses adipogenesis and enhances lipid degradation, even under PON2 knockdown conditions. These results highlight the potential of VUTI as a novel therapeutic approach for obesity by directly targeting adipose tissue to induce fat-specific reduction.

## CRediT authorship contribution statement

**Kamindu Gayashan Marakkalage:** Writing – review & editing, Investigation. **Sang Hyo Kim:** Investigation, Data curation. **Jae Ho Lee:** Investigation, Formal analysis, Data curation. **Hyeong Min Lee:** Writing – original draft, Visualization, Validation, Methodology, Investigation,

Formal analysis, Data curation. **Sang-Ku Yoo:** Writing – review & editing, Supervision, Project administration. **Gu-Choul Shin:** Writing – review & editing, Supervision, Project administration, Funding acquisition, Data curation. **Kwang Pyo Kim:** Writing – review & editing, Data curation. **Hyung Soon Park:** Writing – review & editing, Data curation. **Jihyeon Hur:** Methodology, Formal analysis, Data curation.

## Funding

This study was supported by the National Research Foundation of Korea (NRF) grants, funded by the Korean government (RS-2023-NR076440). The funding agency was not involved in the study design, analysis, or reporting.

## Declaration of Competing Interest

The authors declare the following financial interests/personal relationships which may be considered as potential competing interests: Gu-Choul Shin reports financial support was provided by National Research Foundation of Korea. Sang-Ku Yoo has patent Pyranochromenyl phenol derivative, and pharmaceutical composition for treating metabolic syndrome or inflammatory disease issued to US9783551B2. HML, JHL, SHK, HSP, KGM and S-KY are current employees of Glaceum Inc. and hold its stocks/shares. Glaceum Inc. holds the intellectual property rights of Vutiglabridin. The remaining authors declare no competing interests If there are other authors, they declare that they have no known competing financial interests or personal relationships that could have appeared to influence the work reported in this paper.

## Acknowledgements

The authors gratefully acknowledge the use of services and facilities of Integrative Research Support Center in the Catholic University of Korea.

## Appendix A. Supporting information

Supplementary data associated with this article can be found in the online version at doi:10.1016/j.biopha.2025.118759.

## Data availability

Data will be made available on request.

## References

[1] M. Coelho, T. Oliveira, R. Fernandes, Biochemistry of adipose tissue: an endocrine organ, Arch. Med. Sci. 9 (2) (2013) 191–200.
[2] J. Park, D.M. Euhus, P.E. Scherer, Paracrine and endocrine effects of adipose tissue on cancer development and progression, Endocr. Rev. 32 (4) (2011) 550–570.
[3] P.G. Kopelman, Obesity as a medical problem, Nature 404 (6778) (2000) 635–643.
[4] J.G. Kang, C.Y. Park, Anti-obesity drugs: a review about their effects and safety, Diabetes Metab. J. 36 (1) (2012) 13–25.
[5] J. Jordan, A. Astrup, S. Engeli, K. Narkiewicz, W.W. Day, N. Finer, Cardiovascular effects of phentermine and topiramate: a new drug combination for the treatment of obesity, J. Hypertens. 32 (6) (2014) 1178–1188.
[6] P.M.O. Neil, D.M. Rubino, Exploring the wider benefits of semaglutide treatment in obesity: insight from the STEP program, Post. Med 134 (sup1) (2022) 28–36.
[7] D.H. Ryan, I. Lingvay, J. Deanfield, S.E. Kahn, E. Barros, B. Burguera, H. M. Colhoun, C. Cercato, D. Dicker, D.B. Horn, G.K. Hovingh, O.K. Jeppesen, A. Kokkinos, A.M. Lincoff, S.M. Meyhöfer, T.K. Oral, J. Plutzky, A.P. van Beek, J.P. H. Wilding, R.F. Kushner, Long-term weight loss effects of semaglutide in obesity without diabetes in the SELECT trial, Nat. Med. 30 (7) (2024) 2049–2057.
[8] S. Wharton, R.L. Batterham, M. Bhatta, S. Buscemi, L.N. Christensen, J.P. Frias, E. Jódar, K. Kandler, G. Rigas, T.A. Wadden, W.T. Garvey, Two-year effect of semaglutide 2.4 mg on control of eating in adults with overweight/obesity: STEP 5, Obesity 31 (3) (2023) 703–715.
[9] D.J. Ham, A. Börsch, K. Chojnowska, S. Lin, A.B. Leuchtmann, A.S. Ham, M. Thürkauf, J. Delezie, R. Furrer, D. Burri, M. Sinnreich, C. Handschin, L. A. Tintignac, M. Zavolan, N. Mittal, M.A. Rüegg, Distinct and additive effects of calorie restriction and rapamycin in aging skeletal muscle, Nat. Commun. 13 (1) (2022) 2025.
[10] E. Cava, N.C. Yeat, B. Mittendorfer, Preserving healthy muscle during weight loss, Adv. Nutr. 8 (3) (2017) 511–519.
[11] S.K. Fried, J.O. Hill, M. Nickel, M. DiGirolamo, Prolonged effects of fasting-refeeding on rat adipose tissue lipoprotein lipase activity: influence of caloric restriction during refeeding, J. Nutr. 113 (9) (1983) 1861–1869.
[12] R. Lupoli, E. Lembo, G. Saldalamacchia, C.K. Avola, L. Angrisani, B. Capaldo, Bariatric surgery and long-term nutritional issues, World J. Diabetes 8 (11) (2017) 464–474.
[13] K. Koppo, C. Valle, M. Šiklová-Vítková, E. Czudková, I. de Glisezinski, J. van de Voorde, D. Langin, V. Štich, Expression of lipolytic genes in adipose tissue is differentially regulated during multiple phases of dietary intervention in obese women, Physiol. Res. 62(5) (2013) 527–535.
[14] N. Viguerie, H. Vidal, P. Arner, C. Holst, C. Verdich, S. Avizou, A. Astrup, W. H. Saris, I.A. Macdonald, E. Klimcakova, K. Clément, A. Martinez, J. Hoffstedt, T. I. Sørensen, D. Langin, Adipose tissue gene expression in obese subjects during low-fat and high-fat hypocaloric diets, Diabetologia 48 (1) (2005) 123–131.
[15] M. Karczewska-Kupczewska, A. Nikołajuk, R. Majewski, R. Filarski, M. Stefanowicz, N. Matulewicz, M. Strączkowski, Changes in adipose tissue lipolysis gene expression and insulin sensitivity after weight loss, Endocr. Connect 9 (2) (2020) 90–100.
[16] J.W. Jocken, D. Langin, E. Smit, W.H. Saris, C. Valle, G.B. Hul, C. Holm, P. Arner, E. E. Blaak, Adipose triglyceride lipase and hormone-sensitive lipase protein expression is decreased in the obese insulin-resistant state, J. Clin. Endocrinol. Metab. 92 (6) (2007) 2292–2299.
[17] C. Saponaro, M. Gaggini, F. Carli, A. Gastaldelli, The subtle balance between lipolysis and lipogenesis: a critical point in metabolic homeostasis, Nutrients 7 (11) (2015) 9453–9474.
[18] C. Simmler, G.F. Pauli, S.N. Chen, Phytochemistry and biological properties of glabridin, Fitoterapia 90 (2013) 160–184.
[19] P.A. Belinky, M. Aviram, B. Fuhrman, M. Rosenblat, J. Vaya, The antioxidative effects of the isoflavan glabridin on endogenous constituents of LDL during its oxidation, Atherosclerosis 137 (1) (1998) 49–61.
[20] J.W. Lee, S.S. Choe, H. Jang, J. Kim, H.W. Jeong, H. Jo, K.H. Jeong, S. Tadi, M. G. Park, T.H. Kwak, J. Man Kim, D.H. Hyun, J.B. Kim, AMPK activation with glabridin ameliorates adiposity and lipid dysregulation in obesity, J. Lipid Res. 53 (7) (2012) 1277–1286.
[21] B. Guo, Z. Fang, L. Yang, L. Xiao, Y. Xia, F.J. Gonzalez, L. Zhu, Y. Cao, G. Ge, L. Yang, H. Sun, Tissue and species differences in the glucuronidation of glabridin with UDP-glucuronosyltransferases, Chem. Biol. Inter. 231 (2015) 90–97.
[22] L.S. Choi, I.G. Jo, K.S. Kang, J.H. Im, J. Kim, J. Kim, J.W. Chung, S.K. Yoo, Discovery and preclinical efficacy of HSG4112, a synthetic structural analog of glabridin, for the treatment of obesity, Int J. Obes. (Lond. ) 45 (1) (2021) 130–142.
[23] S.K. Yu, K.K. Suk, K.J. Young, C.J. Wook, I.J. Ho, J.I.G. Yoo, Pyranochromenyl phenol derivative, and pharmaceutical composition for treating metabolic syndrome or inflammatory disease, Glaceum, Inc, Suwon-si, KR, United States, 2017.
[24] E.G. Solon, Autoradiography techniques and quantification of drug distribution, Cell Tissue Res. 360 (1) (2015) 87–107.
[25] P.C. Even, N.A. Nadkarni, Indirect calorimetry in laboratory mice and rats: principles, practical considerations, interpretation and perspectives, Am. J. Physiol. Regul. Integr. Comp. Physiol. 303 (5) (2012) R459–R476.
[26] H. Miyoshi, S.C. Souza, H.H. Zhang, K.J. Strissel, M.A. Christoffolete, J. Kovsan, A. Rudich, F.B. Kraemer, A.C. Bianco, M.S. Obin, A.S. Greenberg, Perilipin promotes hormone-sensitive lipase-mediated adipocyte lipolysis via phosphorylation-dependent and -independent mechanisms, J. Biol. Chem. 281 (23) (2006) 15837–15844.
[27] S. Furukawa, T. Fujita, M. Shimabukuro, M. Iwaki, Y. Yamada, Y. Nakajima, O. Nakayama, M. Makishima, M. Matsuda, I. Shimomura, Increased oxidative stress in obesity and its impact on metabolic syndrome, J. Clin. Investig. 114 (12) (2004) 1752–1761.
[28] H. Heid, S. Rickelt, R. Zimbelmann, S. Winter, H. Schumacher, Y. Dörflinger, Lipid droplets, perilipins and cytokeratins–unravelled liaisons in epithelium-derived cells, PLoS One 8 (5) (2013) e63061.
[29] N. Martinez-Lopez, M. Garcia-Macia, S. Sahu, D. Athonvarangkul, E. Liebling, P. Merlo, F. Cecconi, G.J. Schwartz, R. Singh, Autophagy in the CNS and periphery coordinate lipophagy and lipolysis in the brown adipose tissue and liver, Cell Metab. 23 (1) (2016) 113–127.
[30] G.C. Shin, H.M. Lee, N. Kim, J. Hur, S.K. Yoo, Y.S. Park, H.S. Park, D. Ryu, M. H. Park, J.H. Park, S.U. Seo, L.S. Choi, M.R. Madsen, M. Feigh, K.P. Kim, K.H. Kim, Paraoxonase-2 agonist vutiglabridin promotes autophagy activation and mitochondrial function to alleviate non-alcoholic steatohepatitis, Br. J. Pharm. 181 (19) (2024) 3717–3742.
[31] S. Cinti, G. Mitchell, G. Barbatelli, I. Murano, E. Ceresi, E. Faloia, S. Wang, M. Fortier, A.S. Greenberg, M.S. Obin, Adipocyte death defines macrophage localization and function in adipose tissue of obese mice and humans, J. Lipid Res. 46 (11) (2005) 2347–2355.
[32] H. Lee, Y.J. Lee, H. Choi, E.H. Ko, J.W. Kim, Reactive oxygen species facilitate adipocyte differentiation by accelerating mitotic clonal expansion, J. Biol. Chem. 284 (16) (2009) 10601–10609.
[33] J.P. Castro, T. Grune, B. Speckmann, The two faces of reactive oxygen species (ROS) in adipocyte function and dysfunction, Biol. Chem. 397 (8) (2016) 709–724.
[34] K.V. Tormos, E. Anso, R.B. Hamanaka, J. Eisenbart, J. Joseph, B. Kalyanaraman, N. S. Chandel, Mitochondrial complex III ROS regulate adipocyte differentiation, Cell Metab. 14 (4) (2011) 537–544.

[35] M. Morak, H. Schmidinger, G. Riesenhuber, G.N. Rechberger, M. Kollroser, G. Haemmerle, R. Zechner, F. Kronenberg, A. Hermetter, Adipose triglyceride lipase (ATGL) and hormone-sensitive lipase (HSL) deficiencies affect expression of lipolytic activities in mouse adipose tissues, Mol. Cell Proteom. 11 (12) (2012) 1777–1789.
[36] R. Zechner, P.C. Kienesberger, G. Haemmerle, R. Zimmermann, A. Lass, Adipose triglyceride lipase and the lipolytic catabolism of cellular fat stores, J. Lipid Res. 50 (1) (2009) 3–21.
[37] G. Cildir, S.C. Akıncılar, V. Tergaonkar, Chronic adipose tissue inflammation: all immune cells on the stage, Trends Mol. Med 19 (8) (2013) 487–500.
[38] A. Schäffler, J. Schölmerich, Innate immunity and adipose tissue biology, Trends Immunol. 31 (6) (2010) 228–235.
[39] A. Fernández-Sánchez, E. Madrigal-Santillán, M. Bautista, J. Esquivel-Soto, A. Morales-González, C. Esquivel-Chirino, I. Durante-Montiel, G. Sánchez-Rivera, C. Valadez-Vega, J.A. Morales-González, Inflammation, oxidative stress, and obesity, Int J. Mol. Sci. 12 (5) (2011) 3117–3132.
[40] C. Chrysohoou, D.B. Panagiotakos, C. Pitsavos, I. Skoumas, L. Papademetriou, M. Economou, C. Stefanadis, The implication of obesity on total antioxidant capacity in apparently healthy men and women: the ATTICA study, Nutr. Metab. Cardiovasc Dis. 17 (8) (2007) 590–597.
[41] P.D. Cani, J. Amar, M.A. Iglesias, M. Poggi, C. Knauf, D. Bastelica, A.M. Neyrinck, F. Fava, K.M. Tuohy, C. Chabo, A. Waget, E. Delmée, B. Cousin, T. Sulpice, B. Chamontin, J. Ferrières, J.F. Tanti, G.R. Gibson, L. Casteilla, N.M. Delzenne, M. C. Alessi, R. Burcelin, Metabolic endotoxemia initiates obesity and insulin resistance, Diabetes 56 (7) (2007) 1761–1772.
[42] G.C. Shin, H.M. Lee, N. Kim, S.K. Yoo, H.S. Park, L.S. Choi, K.P. Kim, A.R. Lee, S. U. Seo, K.H. Kim, Paraoxonase-2 contributes to promoting lipid metabolism and mitochondrial function via autophagy activation, Sci. Rep. 12 (1) (2022) 21483.
[43] R. Singh, S. Kaushik, Y. Wang, Y. Xiang, I. Novak, M. Komatsu, K. Tanaka, A. M. Cuervo, M.J. Czaja, Autophagy regulates lipid metabolism, Nature 458 (7242) (2009) 1131–1135.
[44] X. Zhang, D. Wu, C. Wang, Y. Luo, X. Ding, X. Yang, F. Silva, S. Arenas, J. M. Weaver, M. Mandell, V. Deretic, M. Liu, Sustained activation of autophagy suppresses adipocyte maturation via a lipolysis-dependent mechanism, Autophagy 16 (9) (2020) 1668–1682.
[45] A.A. Rahman, A.J. Butcko, E. Songyekutu, J.G. Granneman, E.P. Mottillo, Direct effects of adipocyte lipolysis on AMPK through intracellular long-chain acyl-CoA signaling, Sci. Rep. 14 (1) (2024) 19.
[46] D. Jiang, D. Wang, X. Zhuang, Z. Wang, Y. Ni, S. Chen, F. Sun, Berberine increases adipose triglyceride lipase in 3T3-L1 adipocytes through the AMPK pathway, Lipids Health Dis. 15 (1) (2016) 214.
[47] M. Ahmadian, M.J. Abbott, T. Tang, C.S. Hudak, Y. Kim, M. Bruss, M.K. Hellerstein, H.Y. Lee, V.T. Samuel, G.I. Shulman, Y. Wang, R.E. Duncan, C. Kang, H.S. Sul, Desnutrin/ATGL is regulated by AMPK and is required for a brown adipose phenotype, Cell Metab. 13 (6) (2011) 739–748.
[48] D.G. Hardie, AMP-activated protein kinase as a drug target, Annu Rev. Pharm. Toxicol. 47 (2007) 185–210.
[49] D.M. Shih, Y. Meng, T. Sallam, L. Vergnes, M.L. Shu, K. Reue, P. Tontonoz, A. M. Fogelman, A.J. Lusis, S.T. Reddy, PON2 deficiency leads to increased susceptibility to diet-induced obesity, Antioxidants 8 (1) (2019).
[50] Y. Yang, Y. Zhang, S. Cuevas, V.A. Villar, C. Escano, D.A. L, P. Yu, D.K. Grandy, R. A. Felder, I. Armando, P.A. Jose, Paraoxonase 2 decreases renal reactive oxygen species production, lowers blood pressure, and mediates dopamine D2 receptor-induced inhibition of NADPH oxidase, Free Radic. Biol. Med. 53 (3) (2012) 437–446.
[51] G. Manco, E. Porzio, T.M. Carusone, Human paraoxonase-2 (PON2): protein functions and modulation, Antioxid. (Basel) 10 (2) (2021).
[52] P. Calzadilla, D. Sapochnik, S. Cosentino, V. Diz, L. Dicelio, J.C. Calvo, L.N. Guerra, N-acetylcysteine reduces markers of differentiation in 3T3-L1 adipocytes, Int. J. Mol. Sci. 12 (10) (2011) 6936–6951.
[53] S. Herzig, R.J. Shaw, AMPK: guardian of metabolism and mitochondrial homeostasis, Nat. Rev. Mol. Cell Biol. 19 (2) (2018) 121–135.
[54] O. Göransson, F. Kopietz, M.H. Rider, Metabolic control by AMPK in white adipose tissue, Trends Endocrinol. Metab. 34 (11) (2023) 704–717.
[55] A.J. Garton, S.J. Yeaman, Identification and role of the basal phosphorylation site on hormone-sensitive lipase, Eur. J. Biochem 191 (1) (1990) 245–250.
[56] G.V.N. Kumar, R.S. Wang, A.X. Sharma, N.L. David, T. Amorim, D.S. Sinden, N. K. Doshi, M. Wabitsch, S. Gingras, A. Ejaz, J.P. Rubin, B.A. Maron, P.K. Fazeli, M. L. Steinhauser, Non-canonical lysosomal lipolysis drives mobilization of adipose tissue energy stores with fasting, Nat. Commun. 16 (1) (2025) 1330.